

**Pairing in Degenerate Fermi Gases**

**A THESIS**

*submitted for the Award of Ph. D. degree of*

**MOHANLAL SUKHADIA UNIVERSITY**

*in the*

*Faculty of Science*

*by*

***Salman Ahmed Silotri***



**Under the Supervision of**

**Angom Dilip Kumar Singh, Reader**

**Physical Research Laboratory, Ahmedabad**

**DEPARTMENT OF PHYSICS**

**FACULTY OF SCIENCE**

**MOHANLAL SUKHADIA UNIVERSITY**

**UDAIPUR**

**Year of submission 2010**

# Certificate

*I feel great pleasure in certifying that the thesis entitled "Pairing in Degenerate Fermi Gases" embodies a record of the results of investigations carried out by Silotri Salman Ahmed under my guidance. I am satisfied with the analysis of data, interpretation of results and conclusions drawn.*

*He has completed the residential requirement as per rules.*

*I recommend the submission of thesis.*

Date:

January 28, 2010

Angom Dilip Kumar Singh

Reader

Physical Research Laboratory

Ahmedabad

# Declaration

*I hereby declare that the work incorporated in the present thesis entitled  
"Pairing in Degenerate Fermi Gases " is my own work and is original.  
This work (in part or in full) has not been submitted to any University  
for the award of a Degree or a Diploma.*

Silotri Salman Ahmed Ziya Ahmed

# Acknowledgement

I would like to start by thanking my supervisor Dilip Angom. His continued support and encouragement during my years as a doctoral student has been invaluable and led to the formation of this thesis work. He introduced me to the fascinating field of ultracold atoms and gave me opportunity to work independently.

I owe special gratitude to Hiranmaya Mishra for teaching me thermofield-dynamics techniques which forms the backbone of this thesis work. He shared his invaluable insights improving my understanding of the subject. Discussions with him has always been extremely helpful. In addition, I am grateful to him for careful reading of this thesis and for the incisive feedback.

I also wish to thank Amruta Mishra for her encouragement and collaborating on my first paper. I would also like to thank my course instructors— R. E. Amritkar, V. K. B. Kota, A. Joshipura and S. Ramachandran, P. Venkatakrishnan, J. S. Ray, R. Ramesh, D. Banerjee and U. C. Joshi. The course work experience was very enjoyable with these fine instructors. I am also indebted to S. Mohanty, Bhas Bapat, S. D. Rindani and Utpal Sarkar for their invaluable feedback and advice during my periodical thesis reviews. I also wish to thank P. K. Panigrahi, R. Rangarajan, J. Bhatt, and R. P. Singh for useful discussions and encouragement. I thank all the members of the Theoretical Physics division for maintaining very congenial and informal atmosphere.

I am extremely grateful to Computer Centre and Library staff for their indispensable support and help. Special thanks to P. Sharma, ex-Head academics, for his constant encouragement and support during the initial stages of the thesis. I also thank PRL canteen and administration for their cooperation and services.

There are just too many people and I would like to limit myself to those who one way or the other had direct influence on my life. I would like to thank Latha and Arun for giving enjoyable company and constant support and encouragement. They shared their invaluable experiences making me realize the realities of research life. It is great pleasure to thank my batch-mates Rajesh, Ritesh, Rohit, Akhilesh, Santosh and Ramakrishna for their constant support, concern and long humorous conversations. Without their friendship my years at PRL would not have been as enjoyable. I would also like to thank Manimaran for his company and giving support and advice at the initial stages. I also wish to thank old tea time partners Uma, Sanath, Shreyas, Subimal, Sasadhar, Amit and new night-coffee partner Sumantu for their company and my group members Brajesh and Sandeep for useful discussions. I also thank my officemate Suman and lobby-mate Alok for maintaining peaceful atmosphere at their respective places! Special thanks go to Suman for patiently helping me with his computer skills.

I am thankful to all members of PRL Football Club and all hostel scholars, just too numerous to be mentioned here, for making PRL such a dynamic place. I also thank my college friends for their constant encouragement and concern for my work.

Finally many thanks will always be due to my parents for their love and support and who suffered most during this period due to my absence from home.

# Abstract

The advances in cooling and trapping of atoms present the unique opportunity to study exotic many body phases which were previously elusive in conventional condensed matter systems. In these systems, the interatomic interaction can be tuned via *Feshbach resonances* and the population of each atomic species can be controlled. In this thesis, we study Cooper pairing in two component degenerate atomic Fermi gases. The superfluid systems with matched Fermi surfaces are well described by celebrated Bardeen-Cooper-Schrieffer (BCS) theory. We discuss, in this framework, the crossover from Bardeen-Cooper-Schrieffer (BCS) limit of weakly bound Cooper pairs of fermionic atoms to the Bose-Einstein condensate (BEC) of diatomic molecules as the strength of the interaction is varied. In presence of mismatched Fermi surfaces, however, the system is proposed to admit variety of exotic superfluid phases.

This mismatch can arise due to population imbalance or the mass difference between the two trapped components or both. We, in particular, study the *breached pairing* phase which is potential candidate as a ground state for such imbalanced systems. In this state, excess unpaired fermions occupy the negative quasi-particle energies thereby minimizing the thermodynamic potential. Moreover, it exhibits gapless modes and is also termed as gapless superfluidity.

We consider a variational ground state for the system of nonrelativistic

fermions with a four fermion point interaction to model the phase structure of the ultracold atomic Fermi mixture with equal and unequal population and the mass. We find that *breached pairing* phase with one Fermi surface which admits only one gapless mode, is the stable phase. This rules out the proposal that mass asymmetry between the pairing components can lead to breached pairing with two Fermi surfaces also referred to as *interior gap* state. We also present the temperature effects on these systems within mean field approximation. The temperature effects are taken into account by thermal Bogoliubov transformation. We then extend the formalism from homogeneous system to trapped systems where present day experiments are carried out.

We study equal mass population imbalanced two-component atomic Fermi gas with unequal trap frequencies ( $\omega_{\uparrow} \neq \omega_{\downarrow}$ ) at zero temperature using the local density approximation (LDA). We consider the strongly attracting Bose-Einstein condensation (BEC) limit where polarized (gapless) superfluid, breached pairing phase with one Fermi surface (BP1), is stable. The system exhibits shell structure: unpolarized superfluid  $\rightarrow$  gapless superfluid (BP1)  $\rightarrow$  normal state. Compared to the trap symmetric case, when the majority component is tightly confined the gapless superfluid shell grows in size leading to reduced threshold polarization to form a polarized (gapless) superfluid core. In contrast, when the minority component is tightly confined, we find that the superfluid phase is dominated by the unpolarized superfluid phase with the gapless phase forming a narrow shell. The shell radii for various phases as a function of polarization at different values of trap asymmetry are presented and the features are explained using the phase diagram.

# Table of Contents

<b>Certificate</b>	<b>i</b>
<b>Declaration</b>	<b>ii</b>
<b>Acknowledgement</b>	<b>iii</b>
<b>Abstract</b>	<b>v</b>
<b>List of figures</b>	<b>ix</b>
<b>1 Introduction</b>	<b>2</b>
<b>2 Formalism</b>	<b>10</b>
2.1 Ansatz for the ground state and the Hamiltonian . . . . .	11
2.2 Operator transformation under the Ansatz . . . . .	12
2.3 Effect of temperature . . . . .	15
2.4 Expectation values of the Operators . . . . .	16
2.5 Evaluation of Thermodynamic potential . . . . .	17
2.6 Gap equation . . . . .	19
2.7 Thermodynamic potential and the regularized gap equation .	22
2.8 Stability condition . . . . .	24
2.9 Summary . . . . .	25

<b>3</b>	<b>Superfluid: From BCS to Breached Pairing</b>	<b>28</b>
3.1	Zero temperature limit . . . . .	29
3.2	Dimensionless equations . . . . .	30
3.3	Thermodynamic Potential . . . . .	32
3.4	BCS-BEC Crossover . . . . .	33
3.5	Breached Pair solution . . . . .	36
3.6	Results and Discussions . . . . .	38
3.7	Summary . . . . .	42
<b>4</b>	<b>Trapped Systems</b>	<b>44</b>
4.1	Phase Diagram . . . . .	45
4.2	Trapped Fermions . . . . .	47
4.3	Results and Discussions . . . . .	51
4.4	Summary . . . . .	56
<b>5</b>	<b>Conclusion and Future Directions</b>	<b>59</b>
5.1	Conclusion . . . . .	59
5.2	Future Directions . . . . .	61
	<b>Publications</b>	<b>63</b>
	<b>Bibliography</b>	<b>64</b>

# List of Figures

1.1	The two-channel model for a Feshbach resonance. Atoms which are prepared in the open channel, undergo a collision at low incident energy. In the course of the collision, the open channel is coupled to the closed channel. When a bound state of the closed channel has an energy close to zero, a scattering resonance occurs. Adapted from (1). . . . .	5
3.1	The thermodynamic potential $\Omega$ in units of $E_F k_F^3$ for mass symmetric case at zero-temperature vs $\Delta$ is plotted at $(k_F a)^{-1} = -1$ at fixed chemical potential $\mu = 0.48$ for various values of chemical potential difference $h$ . At $h_0 = 0$ , without chemical potential difference, $\Omega$ has minimum at $\Delta = \Delta_{\text{BCS}}$ corresponding to BCS superfluid. As $h$ is increased, a local minimum appears at $\Delta = 0$ . This local minimum becomes degenerate at $h_c = \Delta/\sqrt{2}$ . Also, a local maximum develops at $\Delta = \Delta_{\text{BP}}$ . For $h > h_3 = \Delta$ , the BCS minimum disappears. . . . .	33
3.2	$\hat{\Delta}$ is plotted against coupling $(k_F a)^{-1}$ at zero temperature without population imbalance. . . . .	34
3.3	$\hat{\nu}$ is plotted against coupling $(k_F a)^{-1}$ at zero temperature without population imbalance. . . . .	36

3.4	The momentum space density profile for mass symmetric case $q = 1$ at (a) $T = 0$ (b) $T = 0.005T_F$ . Here $(k_F a)^{-1} = 2$ and $P = 0.2$ . The profile corresponds to BP1 phase. . . . .	39
3.5	The momentum space density profile for mass symmetric case $q = 1$ at (a) $T = 0$ (b) $T = 0.005T_F$ . Here $(k_F a)^{-1} = 0$ and $P = 0.2$ . The profile corresponds to BP2 phase. This phase, however, is unstable. . . . .	40
3.6	The variation of $\Delta$ against polarization is shown for $m_1/m_2 = 0.15$ at couplings $(k_F a)^{-1} = 0.1$ (dashed) and $(k_F a)^{-1} = 0.5$ (dot-dashed). . . . .	41
3.7	The momentum space density profile for mass asymmetric case $q = 0.15$ at (a) $T = 0$ (b) $T = 0.005T_F$ . Here $q = m_1/m_2$ , $(k_F a)^{-1} = 0.1$ and $P = 0.2$ . The profile corresponds to BP2 phase. This is stable phase. . . . .	42
4.1	The zero temperature phase diagram for $(k_F a)^{-1} = 2.0$ showing unpolarized superfluid (BCS SF), polarized superfluid (BP1), vacuum, and polarized normal (N) phases. The upper (blue) dot denotes the point beyond which the BP1 state ceases to exist. The lower (red) dot represents the tricritical point. The dashed (red) line indicates the second-order transition between the unpolarized SF and BP1 phase. The dot-dashed (black) line indicates the first-order transition between the SF to polarized N state and the BP1 to normal above and below the upper (blue) point, respectively. . . . .	46

- 4.2 (a) The three radii  $R_{f1}$  (outer boundary of unpolarized superfluid),  $R_{TF}$  (outer boundary of BP1 phase) and  $R_{f2}$  (outer boundary of N phase) plotted as a function of polarization  $P$  at trap asymmetry parameter  $\eta = 0$  and  $(k_F a)^{-1} = 2.0$ . (b) The molecular density  $n_m$  and magnetization  $m$  plotted against radius  $r$  measured in units of  $k_F^3$  and  $R_{TF0}$  respectively. . . . . 52
- 4.3 The three radii  $R_{f1}$  (outer boundary of unpolarized superfluid),  $R_{TF}$  (outer boundary of BP1 phase) and  $R_{f2}$  (outer boundary of N phase) plotted as a function of polarization  $P$  for various values of the trap asymmetry parameter  $\eta$ . (a)  $\eta = -0.9$ , (b)  $\eta = -0.5$  (c)  $\eta = 0.5$ , (d)  $\eta = 0.9$ . All the radii are measured in units of  $R_{TF0}$  (outer boundary of superfluid unpolarized cloud). . . . . 54
- 4.4 Density profiles at  $P = 0.65$  for different values of the trap asymmetry parameter  $\eta$ . (a)  $\eta = -0.9$ , (b)  $\eta = -0.5$  (c)  $\eta = 0.5$ , (d)  $\eta = 0.9$ . The molecular density  $n_m$  and the magnetization plotted as a function of radius measured in units of  $k_F^3$  and  $R_{TF0}$  respectively. . . . . 55
- 4.5 The part of phase diagram with the BP1 region enlarged. The solid (red) line indicates the second-order phase transition and dot-dashed (black) line shows first-order transition. Superimposed are the  $\mu$ - $h$  variations as line segments for various values of the trap asymmetry parameter  $\eta$  at  $P = 0.65$ . . . . . 57

## Chapter 1

# Introduction

The ultracold atomic systems provide highly controllable systems to explore the various aspects of the many-body physics. The possibility to control the interaction strength together with variety of trapping configurations, both of magnetic and optical nature, make these systems ideal testing ground to explore exotic and novel many-body phenomena facilitating contact with the ideal conditions of theoretical conjectures. The recent developments along with future directions can be found in (1; 2).

Below a certain critical temperature, Bose systems become Bose-Einstein condensed (BEC) superfluids, with a macroscopic fraction of the particles occupying the lowest single particle mode of the system. With development in the techniques of cooling and trapping of atoms, BEC was finally achieved in 1995 (3; 4). After exploring the condensed bosonic atoms, the search for superfluid transition in ultracold Fermi gases started. The key ingredient in these experiments is to reach quantum degeneracy where thermal de Broglie wavelength  $\lambda_{\text{db}} = \hbar/(2Mk_{\text{B}}T)^{1/2}$  is comparable to interparticl spacing  $n^{-1/3}$  where  $n$  is density of the system.

The microscopic theory explaining the dissipationless flow of current was first formulated by Bardeen, Cooper and Schrieffer (5) based on the work of Cooper (6) referred to as BCS theory. In the BCS theory a degenerate Fermi liquid undergoes pairing instability at a temperature  $T_c \ll E_F$ . The formation of Cooper pairs and their condensation, i.e., macroscopic occupation of

single quantum state occur simultaneously at the transition temperature  $T_c$ .

The BCS theory proposes the non-trivial many body ground state wave-function which below critical temperature admits an energy gap in excitations spectrum. This proposal for the wave-function is based on the work of Cooper (6) who first showed that for an arbitrarily small attractive interaction between two electrons above a filled Fermi sea, a bound state called Cooper pair is formed.

In the conventional theory,  $s$ -wave Cooper pairing occurs between spin-up and spin-down electrons with opposite momenta, and a similar pairing could also be realized with hyperfine states considered to be the two-pseudo-spin component atomic Fermi gas. The statistics of the neutral atom is determined by the number of neutrons in the nucleus since neutral atom contains equal number of proton and electrons. For Fermi atom this neutron number is odd, for example,  $^{40}\text{K}$ ,  $^6\text{Li}$  Alkali atoms have only one electron ( $S = 1/2$ ) out of closed shells. This electron is in a zero orbital angular momentum  $L = 0$  state, and its total angular momentum  $J = L + S$  is  $J = 1/2$ . The nuclear angular momentum  $I$  and electron angular momentum  $J$  are combined in a hyperfine state with total angular momentum  $F = I + J$  giving  $F = I \pm 1/2$  for alkalis. Furthermore, the electron and nuclear spins are coupled by the hyperfine interaction that splits the atomic levels in the absence of magnetic field  $H_{\text{hf}} \propto I \cdot J$ . A weak magnetic field causes Zeeman splitting of the hyperfine levels  $|F, m_F\rangle$  with different  $m_F$ , and atoms trapped in these hyperfine states can be considered to correspond to pseudo-spin labels. Therefore, it is, in principle, possible to study pairing problem in ultracold atomic experiments.

According to Pauli exclusion principle, no two fermions can occupy the same state. This excludes interaction between same hyperfine states requiring two-component system for the singlet pairing. For ultracold regime, the relative kinetic energy between interacting atoms is small unable to surmount the centrifugal barrier due to higher angular momentum states. Only

$s$ -wave scattering is significant which is characterized by the  $s$ -wave scattering length  $a$ .

The standard BCS theory predicts the critical temperature that is exponentially dependent on the inverse of scattering length  $a$ , describing the strength of the interactions between the atoms, as (7)

$$T_c = \frac{8e^{\gamma-2} E_F}{\pi k_B} \exp\left(-\frac{\pi}{2k_F|a|}\right) \quad (1.1)$$

where  $\gamma$  is Euler's constant and  $k_F$  and  $E_F$  are Fermi momentum and energy respectively. Thus critical temperature required to achieve superfluidity is exponentially suppressed and presented major difficulty. In addition, there is no clear experimental signature for the onset of the superfluid phase as there is with bosons (8). The use of Feshbach resonances (9) has solved both of these problems.

The interaction potential between the two atoms depends on their electronic spin states referred to as spin singlet (closed) and spin triplet (open) channel leading to two channel problem. The two colliding atoms are prepared in triplet channel. The threshold of the singlet channel appears above that of the triplet (open) channel. Thus atoms in the closed channel cannot scatter out to large separation. However these channels couple to each other via hyperfine interaction. This produces different Zeeman shifts of the two channels in an external magnetic field. The position of the bound state in closed channel can be tuned with respect to the open channel by varying the magnetic field.

Feshbach resonances appear when the total energy in an open channel matches the energy of a bound state in a closed channel (Fig. 1.1). The two particles in an open channel can scatter to an intermediate state in a closed channel, subsequently decaying to give two particles in the open channel. This second order process, according to perturbation theory, has contribution to scattering length  $a$  proportional to  $(E - E_{\text{res}})^{-1}$ , where  $E$  is the

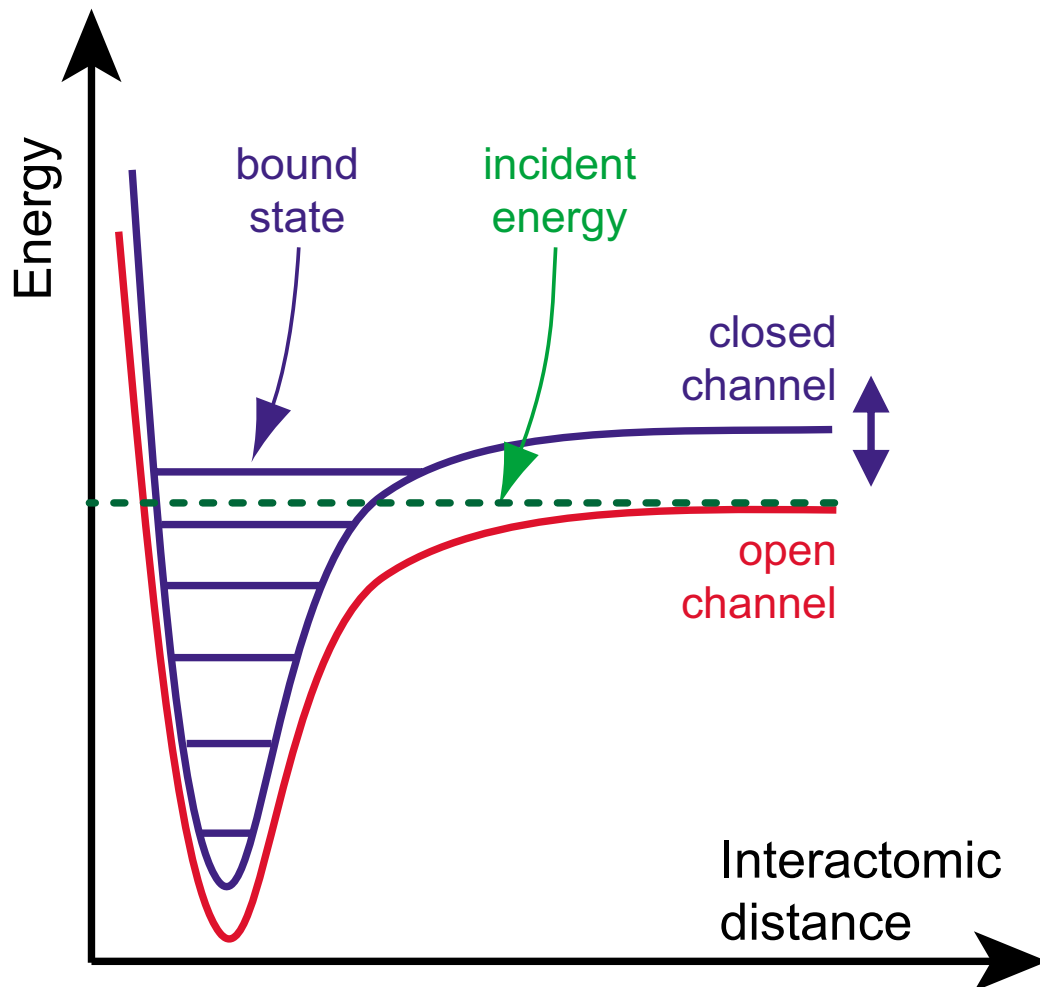


Fig. 1.1: The two-channel model for a Feshbach resonance. Atoms which are prepared in the open channel, undergo a collision at low incident energy. In the course of the collision, the open channel is coupled to the closed channel. When a bound state of the closed channel has an energy close to zero, a scattering resonance occurs. Adapted from (1).

energy of the particles in the open channel and  $E_{\text{res}}$  is energy of the bound state in the closed channel. By changing the magnetic field one can have the bound state in the closed channel just below the continuum threshold in the open channel, in which case  $a$  is negative, to just above it in which  $a$  is positive. The scattering length can be expressed as a function of magnetic field  $B$  (1; 2),

$$a = a_{\text{bg}} \left( 1 - \frac{\Delta B}{B - B_0} \right), \quad (1.2)$$

where  $a_{\text{bg}}$  is the off-resonant background scattering length in the absence of the coupling to the closed channel while  $\Delta B$  and  $B_0$  are the width and position of the resonance.

First quantum degenerate Fermi gas was prepared by De Marco and D. Jin at JILA in 1999 (10) followed by realization of strongly interacting Fermi gases using Feshbach resonance (11; 12). Next on the BEC side  $a > 0$  molecules made of fermions were created and condensed (13; 14; 15; 16; 17). The Bose-Einstein condensation of pairs of Fermionic atoms was achieved (18; 19) followed by observation of quantized vortices on both sides of the Feshbach resonance by Ketterle group at MIT (20) providing convincing proof of superfluidity. In all these experiments equal population of hyperfine states of single species was considered. One can consider the more complex configuration where two components have unequal population as well as different masses.

Within the BCS theory, superfluidity breaks down at the Clogston- Chandrasekhar limit (21; 22) of applied chemical potential difference. However, in imbalanced Fermi mixture the system is expected to show a very interesting and rich phase structure with the appearance of exotic superfluids. These include the existence of breached pairing (23) and Sarma phase (24). It is also possible to have inhomogeneous phases like Larkin-Ovchinnikov-Fulde-Ferrel (LOFF) phase wherein the Cooper pairs have nonzero net momentum (25; 26; 27), superfluidity with deformed Fermi surfaces (28) or a

phase separated state (29). These exotic phases emerge when pairing occurs between two species whose Fermi surfaces do not match. This can happen when the number densities of the two species are different or there is a mismatch in their masses or both.

In a BCS superconductor, mismatch in Fermi momenta can be introduced by applying magnetic field. The applied magnetic field couples not only to the spins but also to orbital motion of the charged conduction electrons. Thus the magnetic field is screened by the orbital motion of the electrons via Meissner effect. However, for sufficiently large magnetic field the energy cost required to expel magnetic field is larger than the condensation energy of the superconducting state. Hence the system makes first order transition to normal state (2; 27). The situation of mismatched Fermi surface with different masses arises in context of color superconductivity in quantum chromodynamics where two different colors of the quarks form condensate. The color superconductivity has implications in astrophysics, e.g., formation of neutron stars and pulsars (27).

The ultracold Fermi gases provide favorable situation to realize superfluid system with mismatch Fermi momenta where population of each component of the mixture can be controlled relating it to chemical potential difference. This is equivalent to applied magnetic field in the BCS superconductor. Recently, series of experiments with population imbalanced systems were performed (30; 31; 32; 33; 34; 35). These experiments led to intense theoretical activity (36; 37; 38; 39; 40; 41; 42; 43; 44; 45; 46; 47; 48; 49; 50; 51).

To date, the two fermion species experiments are with the two hyperfine states of the same alkali atoms forming the condensate. Very recently two fermion species of different masses, lithium and potassium, were laser cooled and trapped to degeneracy (52). Another recent work reports the observations of Feshbach resonances (53) with the same system. Thus achievement of superfluidity with this mass difference could be the next frontier of ongoing experiments in the field of ultracold Fermi gases. Fur-

thermore, the possibility of having equal mass two-component Fermi gas where each component experience different trap frequency were explored in the regime of BCS-BEC crossover (54; 55). Most recently, the Bose-Fermi mixture was realized with two-component system in the BEC regime where breached pairing phase is proposed to be stable (35).

To describe the microscopic physics of a two-component Fermi gas with a Feshbach resonance, in this thesis we use a single-channel model appropriate for *wide* Feshbach resonance relevant to present experimental set-ups. The *wide* and *narrow* Feshbach resonances are distinguished by comparing Fermi wave vector to the length scale associated with the inverse width of the resonance. For the *wide* resonance the condition is given by

$$k_F |R^*| \ll 1. \quad (1.3)$$

The  $R^*$  is the effective range of the interaction intimately connected to the width of the resonance (1; 2). The effective range is defined by

$$k \cot(\delta_0) \simeq -\frac{1}{a} + \frac{1}{2} R^* k^2$$

where  $\delta_0$  is  $s$ -wave phase shift. The *single* channel model describes two species of fermions interacting via a tunable  $s$ -wave interaction whose effective range  $R^*$  is much less than the interparticle distance  $k_F^{-1}$ . At low energies the interaction is thus described by the  $s$ -wave scattering length  $a$ .

The outline of the thesis is as follows. In Chapter 2, we present the formalism to study the superfluid nature of population imbalanced two-component Fermi systems. This formalism is based on the variational ansatz where temperature is taken into account via thermal Bogoliubov transformation.

In Chapter 3, using the formalism developed in Chapter 2, we study breached pairing phase. We first consider the BCS-BEC crossover and then the equal and unequal mass breached pairing phases. We, in particular, focus on  ${}^6\text{Li}$ - ${}^{40}\text{K}$  mixture.

In Chapter 4, we consider the trapped system with isotropic harmonic potential. Starting with the construction of phase diagram in grand canonical ensemble, we derive equations to study trapped system under local density approximation (LDA). We later consider the situation when each trapped hyperfine state experience different trap frequency. The implications of this trap asymmetry are discussed presenting the shell radii of various phases.

Finally, in Chapter 5, we present the conclusion and the possible future directions related to the work presented in the thesis.

## Chapter 2

# Formalism

In this chapter we obtain the expression for the thermodynamic potential using a general pairing ansatz. This ansatz can be modified to calculate thermodynamic potential in more complex situation, for example, Cooper pairing with non-zero center-of-mass momentum. The temperature effect is included under thermal Bogoliubov transformation using the methodology of thermo-field dynamics (TFD) (56; 57; 58; 59; 60). The variational parameters are determined by minimizing the thermodynamic potential. This method has earlier been considered to describe degenerate ultracold fermionic atoms with equal masses for homogeneous (61) as well as inhomogeneous pairing (62). This method has also been applied to relativistic system like cold quark matter and color superconductivity (58; 59; 60).

We first model the fermionic system with a four fermion point interaction and then using the pairing ansatz we obtain the generalized Bogoliubov transformation in Sec. 2.2. Including the effect of temperature in Sec. 2.3, the expectation values of various operators are obtained in this ground state in Sec. 2.4. Using these expectation values we evaluate thermodynamic potential, however, still in terms of variational functions. By functionally minimizing the potential with respect to variational functions, their relation with the thermodynamic quantities are obtained in Sec. 2.6. The thermodynamic potential together with regularized gap equation are presented in Sec 2.7. We then establish the stability condition in Sec. 2.8 and finally summarize

all the important equation together with relevant quantities in Sec. 2.9

## 2.1 Ansatz for the ground state and the Hamiltonian

To examine the superfluidity for Fermionic atoms, we consider a Hamiltonian describing two interacting Fermionic species with four-fermion point interaction given as

$$H = \sum_i \Psi_r^{i\dagger}(\mathbf{z}) \left( -\frac{\hbar^2 \vec{\nabla}^2}{2m_i} \right) \Psi_r^i(\mathbf{z}) + \sum_{r,s} g \Psi_r^{1\dagger}(\mathbf{z}) \Psi_r^1(\mathbf{z}) \Psi_s^{2\dagger}(\mathbf{z}) \Psi_s^2(\mathbf{z}), \quad (2.1)$$

where  $r$  and  $s$  are the spin indices and  $i$  denotes the species with mass  $m_i$ . The constant  $g$  is the bare interaction strength between the two species and is related to the  $s$ -wave scattering length  $a$ . To describe pairing between two different Fermionic species, we consider the ansatz for the ground state (61) of the system as

$$|\Omega\rangle = e^{(B^\dagger - B)} |0\rangle, \quad (2.2)$$

where

$$B^\dagger = \int d\mathbf{k} \epsilon^{ij} \Psi_r^{i\dagger}(\mathbf{k}) f(k) \Psi_{-r}^{j\dagger}(-\mathbf{k}). \quad (2.3)$$

Here  $\epsilon^{ij}$  is the Levi-Cevita tensor, with  $i$  and  $j$  denoting two different Fermionic species. The function  $f(k)$  is the variational function related to the order parameter, as will be seen later. In the case of equal population and for negative weak coupling, this ansatz corresponds to the standard BCS wave function. Clearly the ground states,  $|0\rangle$  and  $|\Omega\rangle$ , are related by the unitary transformation operator  $U = e^{(B^\dagger - B)}$ . Hence the field operators transform as  $\hat{O}' = U \hat{O} U^\dagger$ , where as  $\hat{O}$  is any operator.

## 2.2 Operator transformation under the Ansatz

Now we derive transformation for operators in the new basis in terms of old operators. Specifically let us consider the annihilation operator  $\Psi_s^k$  and define

$$F(\lambda) = e^{\lambda(B^\dagger - B)} \Psi_s^k(\mathbf{q}) e^{-\lambda(B^\dagger - B)}. \quad (2.4)$$

For  $\lambda = 1$  we have <sup>1</sup>

$$\Psi_s^{i'}(\mathbf{q}) = e^{(B^\dagger - B)} \Psi_s^k(\mathbf{q}) e^{-(B^\dagger - B)}. \quad (2.5)$$

Differentiating  $F$  with respect to  $\lambda$ , one obtains

$$F'(\lambda) = e^{\lambda(B^\dagger - B)} [B^\dagger \Psi_s^k(\mathbf{q}) - \Psi_s^k(\mathbf{q}) B^\dagger] e^{-\lambda(B^\dagger - B)}. \quad (2.6)$$

The quantity inside the bracket is evaluated as follows:

consider

$$B^\dagger \Psi_s^k(\mathbf{q}) = \int d\mathbf{k} \epsilon^{ij} \Psi_r^{i\dagger}(\mathbf{k}) f(k) \Psi_{-r}^{j\dagger}(-\mathbf{k}) \Psi_s^k(\mathbf{q}). \quad (2.7)$$

Using

$$\{\Psi_p^a(\mathbf{q}), \Psi_q^{b\dagger}(\mathbf{k})\} = \delta_{pq} \delta_{ab} \delta(\mathbf{q} - \mathbf{k}), \quad (2.8)$$

we obtain

$$B^\dagger \Psi_s^k(\mathbf{q}) = \epsilon^{ik} f(q) \Psi_{-s}^{i\dagger}(-\mathbf{q}) - \epsilon^{kj} f(q) \Psi_{-s}^{j\dagger}(-\mathbf{q}) + \Psi_s^k(\mathbf{q}) B^\dagger \quad (2.9)$$

rearranging the above equation

$$\begin{aligned} B^\dagger \Psi_s^k(\mathbf{q}) - \Psi_s^k(\mathbf{q}) B^\dagger &= \epsilon^{ik} f(q) \Psi_{-s}^{i\dagger}(-\mathbf{q}) + \epsilon^{jk} f(q) \Psi_{-s}^{j\dagger}(-\mathbf{q}) \\ &= 2 \sum_i \epsilon^{ik} f(q) \Psi_{-s}^{i\dagger}(-\mathbf{q}). \end{aligned} \quad (2.10)$$

---

<sup>1</sup>one way to do Campbell-Baker-Hausdorff (CBH) expansion

We use this in the  $F'(\lambda)$  expression, Eq. (2.6), and obtain

$$F'(\lambda) = 2e^{\lambda(B^\dagger - B)} \left[ \sum_i \epsilon^{ik} f(q) \Psi_{-s}^{i\dagger}(-\mathbf{q}) \right] e^{-\lambda(B^\dagger - B)}. \quad (2.11)$$

Now differentiating  $F'(\lambda)$  w.r.t  $\lambda$

$$F''(\lambda) = 2 \sum_i \epsilon^{ik} f(q) e^{\lambda(B^\dagger - B)} \left[ B \Psi_{-s}^{i\dagger}(-\mathbf{q}) - \Psi_{-s}^{i\dagger}(-\mathbf{q}) B \right] e^{-\lambda(B^\dagger - B)}. \quad (2.12)$$

The quantity in the bracket can be evaluated similar to Eq. (2.9). This gives

$$B \Psi_{-s}^{i\dagger}(-\mathbf{q}) - \Psi_{-s}^{i\dagger}(-\mathbf{q}) B = 2 \sum_l \epsilon^{li} f(q) \Psi_s^{l\dagger}(\mathbf{q}). \quad (2.13)$$

This leads to further simplification and we thus obtain

$$F''(\lambda) = 4 \sum_{k,l} \epsilon^{ik} \epsilon^{li} |f(q)|^2 e^{\lambda(B^\dagger - B)} \Psi_s^{l\dagger}(\mathbf{q}) e^{-\lambda(B^\dagger - B)} \quad (2.14)$$

$$\begin{aligned} &= -4 \sum_l \delta_{k,l} |f(q)|^2 e^{\lambda(B^\dagger - B)} \Psi_s^{k\dagger}(\mathbf{q}) e^{-\lambda(B^\dagger - B)} \\ &= -4 |f(q)|^2 e^{\lambda(B^\dagger - B)} \Psi_s^{k\dagger}(\mathbf{q}) e^{-\lambda(B^\dagger - B)} \\ &= -4 |f(q)|^2 F(\lambda). \end{aligned} \quad (2.15)$$

The solution to this equation admits the following form,

$$F(\lambda) = A \cos [2\lambda f(q)] + C \sin [2\lambda f(q)]. \quad (2.16)$$

Next we proceed to calculate the coefficients  $A$  and  $C$ . When  $\lambda = 0$ , we obtain

$$F(0) = A,$$

Now by definition

$$F(\lambda) = e^{\lambda(B^\dagger - B)} \Psi_s^k(\mathbf{q}) e^{-\lambda(B^\dagger - B)},$$

which for  $\lambda = 0$  reduces to

$$F(0) = \Psi_s^k(\mathbf{q}),$$

comparing  $F(0)$  values, we get

$$A = \Psi_s^k(\mathbf{q}). \quad (2.17)$$

Similarly evaluating  $F'(0)$  one obtains

$$C = \epsilon^{ik} \Psi_{-s}^{i\dagger}(-\mathbf{q}). \quad (2.18)$$

The  $F(\lambda)$  can now be written as,

$$F(\lambda) = \Psi_s^k(\mathbf{q}) \cos(2\lambda f(q)) + \epsilon^{ik} \Psi_{-s}^{i\dagger}(-\mathbf{q}) \sin(2\lambda f(q)). \quad (2.19)$$

For  $\lambda = \frac{1}{2}$ ,

$$\Psi_s^{k'}(\mathbf{q}) = \Psi_s^k(\mathbf{q}) \cos(f(q)) + \epsilon^{ik} \Psi_{-s}^{i\dagger}(-\mathbf{q}) \sin(f(q)). \quad (2.20)$$

Renaming the indices we obtain,

$$\Psi_s^{i'}(\mathbf{q}) = \Psi_s^i(\mathbf{q}) \cos(f(q)) - \epsilon^{ij} \Psi_{-s}^{j\dagger}(-\mathbf{q}) \sin(f(q)). \quad (2.21)$$

Similarly

$$\Psi_{-s}^{j'\dagger}(-\mathbf{q}) = \Psi_{-s}^{j\dagger}(-\mathbf{q}) \cos(f(q)) + \epsilon^{ij} \Psi_s^i(\mathbf{q}) \sin(f(q)) \quad (2.22)$$

The two equations can be written as the matrix equation

$$\begin{bmatrix} \Psi_s^{i'}(\mathbf{q}) \\ \Psi_{-s}^{j'\dagger}(-\mathbf{q}) \end{bmatrix} = \begin{bmatrix} \cos(f(q)) & -\epsilon^{ij} \sin(f(q)) \\ \epsilon^{ij} \sin(f(q)) & \cos(f(q)) \end{bmatrix} \begin{bmatrix} \Psi_s^i(\mathbf{q}) \\ \Psi_{-s}^{j\dagger}(-\mathbf{q}) \end{bmatrix}. \quad (2.23)$$

The inverse transformation gives

$$\begin{bmatrix} \Psi_s^i(\mathbf{q}) \\ \Psi_{-s}^{j\dagger}(-\mathbf{q}) \end{bmatrix} = \begin{bmatrix} \cos(f(q)) & \epsilon^{ij} \sin(f(q)) \\ -\epsilon^{ij} \sin(f(q)) & \cos(f(q)) \end{bmatrix} \begin{bmatrix} \Psi_s^{i'}(\mathbf{q}) \\ \Psi_{-s}^{j'\dagger}(-\mathbf{q}) \end{bmatrix}. \quad (2.24)$$

The operators are thus Bogoliubov transformed.

### 2.3 Effect of temperature

To include the effect of temperature and density, we use the method of thermo-field dynamics (TFD) (56; 57; 58; 59; 60) that is particularly useful while dealing with operators and states. Here, the thermal “ground state” is obtained from the zero temperature ground state  $|\Omega\rangle$  through a Bogoliubov transformation in an extended Hilbert space associated with thermal doubling of operators. Explicitly,  $|\Omega, \beta, \mu\rangle$ , the ground state at finite temperature and density is given as

$$|\Omega, \beta, \mu\rangle = \exp(B_{\beta, \mu}^\dagger - B_{\beta, \mu})|\Omega\rangle \quad (2.25)$$

where

$$B_{\beta, \mu}^\dagger = \int [\Psi'(\mathbf{k})^\dagger \underline{\theta}_i(\mathbf{k}, \beta, \mu) \underline{\Psi}'(-\mathbf{k})] d\mathbf{k}. \quad (2.26)$$

In Eq. (2.26), the function  $\theta_i$ , as we shall see later, will be related to the distribution function of the  $i^{\text{th}}$  species and the underlined operators are the operators in the extended Hilbert space associated with thermal doubling. Let us note that the ansatz for the thermal ground state as in Eq. (2.25) is obtained from the perturbative vacuum  $|0\rangle$  by two successive Bogoliubov transformations. In the description of the ground state we have three functions, the condensate function  $f(k)$  and the two thermal function  $\theta_i(\mathbf{k}, \beta)$  ( $i = 1, 2$ ). All these ansatz functions shall be determined through variational principle i.e. through an extremization of thermodynamic potential  $\Omega = T + V - s/\beta - \mu\rho$  which is the relevant quantity to be extremized for finite temperature. Let us

note that, with the state defined as in Eq. (2.25), the expectation value for the number operator, for example, is given as

$$\langle \Omega, \beta, \mu | \Psi_r^{a'\dagger}(\mathbf{k}_1) \Psi_s^{b'}(\mathbf{k}_2) | \Omega, \beta, \mu \rangle = \sin^2(\theta_a(k)) \delta_{rs} \delta_{ab} \delta(\mathbf{k}_1 - \mathbf{k}_2). \quad (2.27)$$

We henceforth use the notation  $\langle \Omega, \beta, \mu | G | \Omega, \beta, \mu \rangle \leftrightarrow \langle G \rangle$

We also note that we are not using anywhere any perturbative technique using propagators and expansion in any coupling, however, the approximation lies in the ansatz for the ground state. As we shall see later, such an ansatz corresponds to the meanfield approximation.

## 2.4 Expectation values of the Operators

Noting that the variational state in Eq. (2.25) arises from successive Bogoliubov transformations, one can calculate the expectation values of the various operators using Eq. (2.24) and Eq. (2.27). With  $\langle \hat{O} \rangle$  representing the expectation value of an operator  $\hat{O}$  in the new ground state of the system  $\langle \Omega, \beta, \mu | \hat{O} | \Omega, \beta, \mu \rangle$ , we thus have

$$\begin{aligned} \langle \Omega | \Psi_r^{1\dagger}(\mathbf{k}_1) \Psi_s^1(\mathbf{k}_2) | \Omega \rangle &= \left\langle \left( \Psi_r^{1\dagger}(\mathbf{k}_1) \cos(f(k_1)) + \Psi_{-r}^2(-\mathbf{k}_1) \sin(f(k_1)) \right) \cdot \right. \\ &\quad \left. \left( \Psi_s^1(\mathbf{k}_2) \cos(f(k_2)) + \Psi_{-s}^{2\dagger}(-\mathbf{k}_2) \sin(f(k_2)) \right) \right\rangle \\ &= \cos^2(f(k_1)) \delta_{rs} \delta(\mathbf{k}_1 - \mathbf{k}_2) \sin^2(\theta_1(k_1)) + \\ &\quad \sin^2(f(k_1)) \delta_{rs} \delta(\mathbf{k}_1 - \mathbf{k}_2) \cos^2(\theta_2(k_1)). \quad (2.28) \end{aligned}$$

Similarly, one obtains

$$\begin{aligned} \langle \Psi_r^{1\dagger}(\mathbf{k}_1) \Psi_s^1(\mathbf{k}_2) \rangle &= [\cos^2(f(k_1)) \sin^2(\theta_1(k_1)) + \sin^2(f(k_1)) \\ &\quad \cos^2(\theta_2(k_1))] \delta_{rs} \delta(\mathbf{k}_1 - \mathbf{k}_2), \end{aligned} \quad (2.29)$$

$$\begin{aligned} \langle \Psi_r^{2\dagger}(\mathbf{k}_1) \Psi_s^2(\mathbf{k}_2) \rangle &= [\cos^2(f(k_1)) \sin^2(\theta_2(k_1)) - \sin^2(f(k_1)) \\ &\quad \cos^2(\theta_1(k_1))] \delta_{rs} \delta(\mathbf{k}_1 - \mathbf{k}_2), \end{aligned} \quad (2.30)$$

$$\begin{aligned} \langle \Psi_r^1(\mathbf{k}_1) \Psi_s^2(\mathbf{k}_2) \rangle &= -\frac{\sin(2f(k_1))}{2} [1 - \sin^2(\theta_1(k_1)) \\ &\quad - \sin^2(\theta_2(k_1))] \delta_{r-s} \delta(\mathbf{k}_1 + \mathbf{k}_2), \end{aligned} \quad (2.31)$$

$$\begin{aligned} \langle \Psi_r^{1\dagger}(\mathbf{k}_1) \Psi_s^{2\dagger}(\mathbf{k}_2) \rangle &= \frac{\sin(2f(k_1))}{2} [1 - \sin^2(\theta_1(k_1)) \\ &\quad - \sin^2(\theta_2(k_1))] \delta_{r-s} \delta(\mathbf{k}_1 + \mathbf{k}_2). \end{aligned} \quad (2.32)$$

## 2.5 Evaluation of Thermodynamic potential

The thermodynamic potential density  $\Omega$  is given by

$$\Omega = T + V - \frac{s}{\beta} - \mu_i \rho_i, \quad (2.33)$$

where  $T$  and  $V$  as the kinetic and potential energy contributions respectively,  $s$  is the entropy density and  $\mu_i$  is the chemical potential for the species ' $i$ '.

Now each term in the Hamiltonian can be calculated, for example

$$\begin{aligned} \langle \Omega | T - \mu_i \hat{N}_i | \Omega \rangle &= \sum_{a=1,2} \sum_{r,s} \langle \Omega | \Psi_r^{a\dagger}(\mathbf{z}) (\varepsilon_a - \mu_a) \Psi_s^a(\mathbf{z}) | \Omega \rangle \\ &= \left[ \langle \Psi^{1\dagger}(\mathbf{z}) (\varepsilon_1 - \mu_1) \Psi^1(\mathbf{z}) \rangle + \langle \Psi^{2\dagger}(\mathbf{z}) (\varepsilon_2 - \mu_2) \Psi^2(\mathbf{z}) \rangle \right] \end{aligned} \quad (2.34)$$

where we have defined the number operator  $\hat{N}_i = \Psi^{i\dagger} \Psi^i$  with kinetic energy of each particle given by

$$\varepsilon_i = \frac{\hbar^2 k_i^2}{2m_i} \quad (2.35)$$

This gives

$$\begin{aligned}
\langle \Omega | T - \mu_i \hat{N}_i | \Omega \rangle &= \left( \frac{1}{2\pi} \right)^3 \int d^3 k_1 (\varepsilon_1 - \mu_1) [\cos^2 (f (k_1)) \sin^2 (\theta_1 (k_1)) \\
&\quad + \sin^2 (f (k_1)) \cos^2 (\theta_2 (k_1))] \\
&\quad + \left( \frac{1}{2\pi} \right)^3 \int d^3 k_2 (\varepsilon_2 - \mu_2) [\cos^2 (f (k_1)) \sin^2 (\theta_2 (k_1)) \\
&\quad + \sin^2 (f (k_1)) \cos^2 (\theta_1 (k_1))] . \tag{2.36}
\end{aligned}$$

Consider the potential term due to interparticle interaction,

$$\langle \Omega | V | \Omega \rangle = \left\langle \Omega \left| \sum_{p,q,r,s} g \Psi_p^{1\dagger}(\mathbf{z}) \Psi_q^1(\mathbf{z}) \Psi_r^{2\dagger}(\mathbf{z}) \Psi_s^2(\mathbf{z}) \right| \Omega \right\rangle . \tag{2.37}$$

By applying Wick's theorem,

$$\begin{aligned}
\langle \Omega | V | \Omega \rangle &= g \sum_{p,q,r,s} \langle \Psi_p^{1\dagger}(\mathbf{z}) \Psi_r^1(\mathbf{z}) \rangle \langle \Psi_q^{2\dagger}(\mathbf{z}) \Psi_s^2(\mathbf{z}) \rangle \\
&\quad - g \sum_{p,q,r,s} \langle \Psi_p^{1\dagger}(\mathbf{z}) \Psi_q^{2\dagger}(\mathbf{z}) \rangle \langle \Psi_r^1(\mathbf{z}) \Psi_s^2(\mathbf{z}) \rangle \\
&= g \rho_1 \rho_2 + g I_D^2, \tag{2.38}
\end{aligned}$$

where we have defined the densities as

$$\begin{aligned}
\rho_1 &= \langle \Psi_r^{1\dagger}(\mathbf{k}) \Psi_s^1(\mathbf{k}) \rangle \\
&= \left( \frac{1}{2\pi} \right)^3 \int d^3 k [\cos^2 (f (k)) \sin^2 (\theta_1 (k)) + \sin^2 (f (k)) \cos^2 (\theta_2 (k))] , \tag{2.39}
\end{aligned}$$

$$\begin{aligned}
\rho_2 &= \langle \Psi_r^{2\dagger}(\mathbf{k}) \Psi_s^2(\mathbf{k}) \rangle \\
&= \left( \frac{1}{2\pi} \right)^3 \int d^3 k [\cos^2 (f (k)) \sin^2 (\theta_2 (k)) + \sin^2 (f (k)) \cos^2 (\theta_1 (k))] , \tag{2.40}
\end{aligned}$$

$$\begin{aligned}
I_D &= \langle \Psi_r^1(\mathbf{k}) \Psi_s^2(-\mathbf{k}) \rangle \\
&= \left( \frac{1}{2\pi} \right)^3 \int d^3k \frac{\sin(2f(k))}{2} [1 - \sin^2(\theta_1(k)) - \sin^2(\theta_2(k))].
\end{aligned} \tag{2.41}$$

Entropy density is defined as

$$s = - \sum_{i=1,2} \left( \frac{1}{2\pi} \right)^3 \int d^3k [n_i \log(n_i) + (1 - n_i) \log(1 - n_i)], \tag{2.42}$$

where

$$n_i = \sin^2(\theta_i(k)), \tag{2.43}$$

is the occupation function of the  $i^{\text{th}}$  species. Thus each term of the thermodynamic potential density Eq. (2.33) is evaluated as a functional of  $f(k)$  and  $\theta_i(k, \beta)$  using Eq. (2.36), (2.38), (2.39), (2.40), (2.41), (2.42).

## 2.6 Gap equation

To find the gap equation, the thermodynamic functional  $\Omega(f(k), \theta_1, \theta_2)$ , Eq. (2.33), is minimized with respect to  $f(k)$ . This gives

$$\tan[2f(k)] = - \frac{2gI_D}{[(\varepsilon_1 - \mu_1) + (\varepsilon_2 - \mu_2)] + g\rho_1 + g\rho_2}. \tag{2.44}$$

We define chemical potentials with mean field correction,

$$\nu_i = \mu_i - g\rho_j | \epsilon^{ij} |. \tag{2.45}$$

Using the above definition,

$$\tan(2f(k)) = - \frac{2gI_D}{[(\varepsilon_1 - \nu_1) + (\varepsilon_2 - \nu_2)]} \tag{2.46}$$

$$\tan(2f(k)) = - \frac{gI_D}{(\varepsilon - \nu)}, \tag{2.47}$$

where in the last equation we define the average kinetic energy,

$$\varepsilon = \frac{\varepsilon_1 + \varepsilon_2}{2}, \quad (2.48)$$

and average chemical potential (with mean field correction),

$$\nu = \frac{\nu_1 + \nu_2}{2}. \quad (2.49)$$

This leads to

$$\tan(2f(k)) = \frac{\Delta}{(\varepsilon - \nu)}. \quad (2.50)$$

where we have defined order parameter or gap as

$$\Delta = -gI_D \quad (2.51)$$

Then using the definition of  $I_D$  from Eq. (2.41), we obtain

$$\Delta = -g \left( \frac{1}{2\pi} \right)^3 \int d^3k \frac{\sin(2f(k))}{2} [1 - \sin^2(\theta_1(k)) - \sin^2(\theta_2(k))] \quad (2.52)$$

Using Eq. (2.50), it simplifies to

$$\Delta = -g \left( \frac{1}{2\pi} \right)^3 \int d^3k \frac{\Delta}{2\sqrt{(\varepsilon - \nu)^2 + \Delta^2}} [1 - \sin^2(\theta_1(k)) - \sin^2(\theta_2(k))]. \quad (2.53)$$

The variational parameter  $\theta_i$ , related to temperature effect, is determined by the condition

$$\delta\langle\Omega\rangle/\delta\theta_i(k) = 0. \quad (2.54)$$

This equation, for  $\theta_1$ , leads to

$$-\frac{1}{\beta} \sin(2\theta_1(k)) \log(\tan^2(\theta_1(k))) = (\varepsilon_1 - \nu_1) \cos^2(f(k)) - (\varepsilon_2 - \nu_2) \sin^2(f(k)). \quad (2.55)$$

Rewriting the equation

$$\begin{aligned}
-\frac{1}{\beta} \sin [2\theta_1 (k)] \log [\tan^2 (\theta_1 (k))] &= (\varepsilon_1 - \nu_1) \cos^2 (f (k)) \\
&\quad - (\varepsilon_2 - \nu_2) \sin^2 (f (k)) \\
&= \frac{1}{2} [(\varepsilon_1 - \nu_1) - (\varepsilon_2 - \nu_2)] + \sqrt{(\varepsilon - \nu)^2 + \Delta^2},
\end{aligned} \tag{2.56}$$

where in the second equality, we have used Eq. (2.50). This equation can now be written as

$$\log [\tan^2 (\theta_1 (k))] = -\beta\omega_1 \tag{2.57}$$

$$\tan^2 (\theta_1 (k)) = \exp (-\beta\omega_1) \tag{2.58}$$

where we have introduced the following quantities

$$\begin{aligned}
\omega_1 &= \omega + \delta_\xi \\
\omega &= \sqrt{\xi^2 + \Delta^2}
\end{aligned} \tag{2.59}$$

$$\delta_\xi = \frac{1}{2} [(\varepsilon_1 - \nu_1) - (\varepsilon_2 - \nu_2)] \tag{2.60}$$

$$\xi = \varepsilon - \nu \tag{2.61}$$

Here  $\omega_1$  represent quasi-particle energy for component with mass  $m_1$  with  $\omega$  as standard BCS quasiparticle energy in absence of mismatch Fermi momenta. The  $\delta_\xi$  measures the difference between the kinetic energy of the two components with respects to their chemical potentials  $\nu_i$  and  $\xi$  measures the average kinetic energy with respect to average chemical potential. Following from Eq. (2.58), density distribution for the component of the type 1 is,

$$\begin{aligned}
n_1 (\omega_1) &= \sin^2 (\theta_1 (k)) \\
&= \frac{1}{\exp (\beta\omega_1) + 1}
\end{aligned} \tag{2.62}$$

Now similarly one can obtain for the other component,

$$\omega_2 = \omega - \delta_\xi$$

with distribution function,

$$\begin{aligned} n_2(\omega_2) &= \sin^2(\theta_2(k)) \\ &= \frac{1}{\exp(\beta\omega_2) + 1} \end{aligned} \quad (2.63)$$

Thus the quasiparticles follow Fermi-Dirac statistics with energies  $\omega_i$ . It should be noted that depending on the value of  $\delta_\xi$  the quasiparticle energies  $\omega_i$  can vanish leading to the gapless modes. This gapless phase will be discussed in the Chapter 3.

## 2.7 Thermodynamic potential and the regularized gap equation

We have now determined for the variational parameters  $f(k)$  (Eq. (2.50)) and  $\theta_i$  (Eq. (2.62), (2.63)). This leads to the following expression for thermodynamic potential in the paired state under the proposed pairing ansatz,

$$\begin{aligned} \Omega &= \frac{1}{(2\pi)^3} \int d^3k \left[ \xi - \omega - \frac{1}{\beta} \sum_i \ln(1 + \exp(-\beta\omega_i)) \right] \\ &\quad - \frac{\Delta^2}{g}. \end{aligned} \quad (2.64)$$

The number density and gap equation can now be directly obtained through relations,

$$0 = \frac{\partial \Omega}{\partial \Delta}, \quad (2.65)$$

$$\rho_1 = -\frac{\partial \Omega}{\partial \mu_1}, \quad (2.66)$$

$$\rho_2 = -\frac{\partial \Omega}{\partial \mu_2}. \quad (2.67)$$

The densities for the two fermion species are then given by

$$\begin{aligned} \rho_1 &= \frac{1}{(2\pi)^3} \int d^3k \left[ \frac{1}{2} \left( 1 + \frac{\xi}{\omega} \right) \sin^2(\theta_1) \right. \\ &\quad \left. + \frac{1}{2} \left( 1 - \frac{\xi}{\omega} \right) \cos^2(\theta_2) \right], \end{aligned} \quad (2.68)$$

$$\begin{aligned} \rho_2 &= \frac{1}{(2\pi)^3} \int d^3k \left[ \frac{1}{2} \left( 1 + \frac{\xi}{\omega} \right) \sin^2(\theta_2) \right. \\ &\quad \left. + \frac{1}{2} \left( 1 - \frac{\xi}{\omega} \right) \cos^2(\theta_1) \right]. \end{aligned} \quad (2.69)$$

The gap equation for nonzero  $\Delta$  is given by

$$-\frac{1}{g} = \frac{1}{(2\pi)^3} \int d^3k \frac{1}{2\omega} [1 - \sin^2(\theta_1) - \sin^2(\theta_2)]. \quad (2.70)$$

This equation is ultraviolet divergent which is characteristic of the contact interaction. It is rectified by subtracting the vacuum contribution, i.e., by subtracting out  $T = 0$  and  $\nu = 0$  contribution from the gap equation and relating this renormalized coupling to the  $s$ -wave scattering length  $a$  (63; 61).

Thus the regularized gap equation is

$$-\frac{\tilde{m}}{2\pi\hbar^2 a} = \frac{1}{(2\pi)^3} \int d^3k \left( \frac{1}{2\omega} [1 - \sin^2(\theta_1) - \sin^2(\theta_2)] - \frac{1}{2\varepsilon_k} \right), \quad (2.71)$$

where  $\tilde{m}$  is the reduced mass defined as,

$$\frac{1}{\tilde{m}} = \frac{1}{m_1} + \frac{1}{m_2} \quad (2.72)$$

## 2.8 Stability condition

The stability of the pairing state is decided by comparing the thermodynamic potential of the superconducting matter with that of the normal matter. Thus the relevant quantity is the difference of the thermodynamic potential between the paired and normal phases. The thermodynamic potential of the paired Fermionic mixture is

$$\Omega = \frac{1}{(2\pi)^3} \int d^3k \left[ \xi - \omega - \frac{1}{\beta} \sum_i \ln(1 + \exp(-\beta\omega_i)) \right] - \frac{\Delta^2}{g}. \quad (2.73)$$

Subtracting the thermodynamic potential for normal matter ( $\Delta = 0$ ) from the above equation, we have the difference in the thermodynamic potential between the condensed and the normal matter as

$$\delta\Omega = \frac{1}{(2\pi)^3} \int d^3k \left[ |\xi| - \omega - \frac{1}{\beta} \sum_i \ln(1 + \exp(-\beta\omega_i)) + \frac{1}{\beta} \sum_i \ln(1 + \exp(-\beta\omega_{0i})) \right] - \frac{\Delta^2}{g}. \quad (2.74)$$

Here  $\omega_i = \omega \pm \delta_\xi$  and  $\omega_{0i} = |\xi| \pm \delta_\xi$ . This difference in the thermodynamic potential,  $\delta\Omega$  has to be negative for the stability of the paired state. Further one can use the gap equation to eliminate the coupling  $g$  in Eq. (2.74) to

obtain

$$\begin{aligned} \delta\Omega = & \frac{1}{(2\pi)^3} \int d^3k \left[ |\xi| - \omega + \frac{\Delta^2}{2\omega} - \frac{1}{\beta} \sum_i \ln(1 + \exp(-\beta\omega_i)) \right. \\ & \left. + \frac{1}{\beta} \sum_i \ln(1 + \exp(-\beta\omega_{0i})) - \frac{\Delta^2}{2\omega} [\sin^2(\theta_1) + \sin^2(\theta_2)] \right]. \end{aligned} \quad (2.75)$$

This expression is free of ultraviolet divergence and will be used to determine the stability of the given paired state. It should be noted that  $\sin^2(\theta_i)$  are quasiparticle distribution function with energies  $\omega_i$ .

## 2.9 Summary

Here we write the final set of equations: the thermodynamic potential for the pairing state

$$\Omega = \frac{1}{(2\pi)^3} \int d^3k \left[ \xi - \omega - \frac{1}{\beta} \sum_i \ln(1 + \exp(-\beta\omega_i)) \right] - \frac{\Delta^2}{g}. \quad (2.76)$$

The thermodynamic potential difference

$$\begin{aligned} \delta\Omega = & \frac{1}{(2\pi)^3} \int d^3k \left[ |\xi| - \omega + \frac{\Delta^2}{2\omega} - \frac{1}{\beta} \sum_i \ln(1 + \exp(-\beta\omega_i)) \right. \\ & \left. + \frac{1}{\beta} \sum_i \ln(1 + \exp(-\beta\omega_{0i})) - \frac{\Delta^2}{2\omega} [\sin^2(\theta_1) + \sin^2(\theta_2)] \right]. \end{aligned} \quad (2.77)$$

The regularized gap equation

$$-\frac{\tilde{m}}{2\pi\hbar^2 a} = \frac{1}{(2\pi)^3} \int d^3k \left( \frac{1}{2\omega} [1 - \sin^2(\theta_1) - \sin^2(\theta_2)] - \frac{1}{2\varepsilon_k} \right), \quad (2.78)$$

and total and difference number densities

$$\begin{aligned}\rho &= \frac{1}{(2\pi)^3} \int d^3k \left[ \frac{1}{2} \left( 1 + \frac{\xi}{\omega} \right) (\sin^2(\theta_1) + \cos^2(\theta_1)) \right. \\ &\quad \left. + \frac{1}{2} \left( 1 - \frac{\xi}{\omega} \right) (\sin^2(\theta_2) + \cos^2(\theta_2)) \right], \\ \delta_\rho &= \frac{1}{(2\pi)^3} \int d^3k [\sin^2(\theta_1) - \sin^2(\theta_2)]\end{aligned}\quad (2.79)$$

Let us consider,

$$\delta_\xi = \frac{1}{2} [(\varepsilon_1 - \nu_1) - (\varepsilon_2 - \nu_2)] \quad (2.80)$$

introducing

$$\delta_\nu = \frac{1}{2}(\nu_1 - \nu_2) \quad (2.81)$$

and mass ratio

$$q = \frac{m_1}{m_2} \quad (2.82)$$

the  $\delta_\xi$  can be written as

$$\delta_\xi = \frac{1-q}{1+q}\xi - \delta_\nu \quad (2.83)$$

Thus the related quantities are

$$\omega_1 = \omega + \delta_\xi, \quad (2.84)$$

$$\omega = \sqrt{\xi^2 + \Delta^2}, \quad (2.85)$$

$$\delta_\xi = \frac{1-q}{1+q}\varepsilon - \delta_\nu, \quad (2.86)$$

$$\xi = \varepsilon - \nu. \quad (2.87)$$

To study the system, the coupling strength ( characterized by the scattering length  $a$ ) and densities of each component  $\rho_i$  are specified. Solving the gap, Eq. (2.78), and the density equations, Eq. (2.79), self consistently then the order parameter  $\Delta$  and chemical potential for each component  $\nu_i$  are obtained. The solution thus obtained is used to calculate thermodynamic potential difference  $\delta\Omega$  in Eq. (2.77) to determine which phase has lower

thermodynamic potential and hence stable.

## Chapter 3

# Superfluid: From BCS to Breached Pairing

In this chapter we mainly focus on breached pair phase in homogeneous system. This phase describe the polarized superfluid where superfluidity persists together with population imbalance. The normal and superfluid phase separate in momentum space but forming homogeneous mixture in real space.

Using the equations derived in previous chapter, we first consider the situation in zero temperature limit in Sec. 3.1 which later will be useful for studying breached pair phase. Expressing the various quantities in dimensionless units we characterize the system by universal dimensionless parameters in Sec. 3.2. The evolution of BCS state is presented in Sec. 3.3 followed by discussions on BCS-BEC crossover in Sec. 3.4. Finally we discuss the breached pair phase in Sec. 3.5. We are presented with two breached pairing phases: breached pairing with two Fermi surfaces (BP2) and breached pairing with one Fermi surface (BP1). We explore which one of these two phases is stable for equal and unequal mass cases. Finally, we summarize our results in Sec. 3.7

### 3.1 Zero temperature limit

At finite temperature, the pairing ansatz description is equivalent to mean-field treatment and thus unreliable at temperature comparable to transition temperature  $T_C$  at which order parameter  $\Delta$  vanishes. The zero temperature treatment thus avoids thermal fluctuation and simplifies the mathematical description giving clear understanding of the breached pairing phase.

In the limit of zero temperature, the quasi-particle distribution of each atomic species is given by

$$n_i(k) = \lim_{\beta \rightarrow \infty} \frac{1}{\exp(\beta\omega_i) + 1} = \Theta(-\omega_i), \quad (3.1)$$

where  $\Theta(\dots)$  is the Heaviside step function. The gap equation in this limit is

$$-\frac{\tilde{m}}{2\pi\hbar^2 a} = \frac{1}{(2\pi)^3} \int d^3k \left[ \frac{1}{2\omega} (1 - \Theta(-\omega_1) - \Theta(-\omega_2)) - \frac{1}{2\varepsilon_k} \right].$$

The densities of the two atomic species are

$$\begin{aligned} \rho_1 &= \frac{1}{(2\pi)^3} \int d^3k \left[ \frac{1}{2} \left( 1 + \frac{\xi}{\omega} \right) \Theta(-\omega_1) \right. \\ &\quad \left. + \frac{1}{2} \left( 1 - \frac{\xi}{\omega} \right) (1 - \Theta(-\omega_2)) \right], \end{aligned} \quad (3.2)$$

$$\begin{aligned} \rho_2 &= \frac{1}{(2\pi)^3} \int d^3k \left[ \frac{1}{2} \left( 1 + \frac{\xi}{\omega} \right) \Theta(-\omega_2) \right. \\ &\quad \left. + \frac{1}{2} \left( 1 - \frac{\xi}{\omega} \right) (1 - \Theta(-\omega_1)) \right]. \end{aligned} \quad (3.3)$$

The total density and difference equation in this limit are given by

$$\rho = \frac{1}{(2\pi)^3} \int d^3k \left[ 1 - \frac{\xi}{\omega} (1 - \Theta(-\omega_1) - \Theta(-\omega_2)) \right], \quad (3.4)$$

$$\delta_\rho = \frac{1}{(2\pi)^3} \int d^3k [\Theta(-\omega_1) - \Theta(-\omega_2)], \quad (3.5)$$

and thermodynamic potential density Eq. (2.76) can be expressed as

$$\Omega = \frac{1}{(2\pi)^3} \int d^3k [\xi - \omega + \omega_1 \Theta(-\omega_1) + \omega_2 \Theta(-\omega_2)] - \frac{\Delta^2}{g} \quad (3.6)$$

where we have made use of the following identity:

$$\lim_{x \rightarrow \infty} \frac{1}{a} \ln(1 + e^{-ax}) = x \Theta(-x). \quad (3.7)$$

### 3.2 Dimensionless equations

We express the thermodynamic potential, gap, number density equation in dimensionless units amenable for numerical investigation. To this end, we use the Fermi energy,

$$E_F = \frac{\hbar^2 k_F^2}{2\tilde{m}}, \quad (3.8)$$

as convenient energy scale where  $k_F$  is corresponding Fermi momentum. To proceed further we define,

$$k_F^3 = 6\pi^2(\rho_1 + \rho_2) \quad (3.9)$$

$$= 6\pi^2(\rho) \quad (3.10)$$

and

$$E_F = k_B T_F \quad (3.11)$$

introducing Fermi temperature  $T_F$ . Defining

$$x = \frac{k}{k_F}, \quad (3.12)$$

the average kinetic energy  $\varepsilon$  can be calculated as follows: by definition,

$$\begin{aligned}\varepsilon &= \frac{1}{2}(\varepsilon_1 + \varepsilon_2) \\ &= \frac{\hbar^2 k^2}{4} \left( \frac{1}{m_1} + \frac{1}{m_2} \right) \\ &= \frac{\hbar^2 k^2}{4\tilde{m}}.\end{aligned}\tag{3.13}$$

Now dividing both sides by  $E_F$  and using Eq. (3.8) and Eq. (3.12),

$$\frac{\varepsilon}{E_F} = \frac{x^2}{2}.\tag{3.14}$$

We define the following set of normalized or dimensionless quantities,

$$\hat{\Delta} = \frac{\Delta}{E_F},\tag{3.15}$$

$$\hat{\nu} = \frac{\nu}{E_F},\tag{3.16}$$

$$\hat{\delta}_\nu = \frac{\delta_\nu}{E_F},\tag{3.17}$$

$$\hat{\omega}_i = \frac{\omega_i}{E_F},\tag{3.18}$$

$$\hat{\Omega} = \frac{\Omega}{E_F^{5/2}}.\tag{3.19}$$

$$\tag{3.20}$$

This transforms the equations in the following dimensionless forms:

Gap equation

$$-\frac{\pi}{k_F a} = \int_0^\infty x^2 dx \left[ \frac{1}{\hat{\omega}} (1 - n(\hat{\omega}_1) - n(\hat{\omega}_2)) - \frac{1}{\hat{\varepsilon}} \right].\tag{3.21}$$

The total density equation,

$$\frac{2}{3} = \int x^2 dx \left[ 1 - \frac{\hat{\xi}}{\hat{\omega}} (1 - n(\hat{\omega}_1) - n(\hat{\omega}_2)) \right].\tag{3.22}$$

We define the *Polarization*  $P$  measuring relative population of the two component.

$$P = \frac{\delta_\rho}{\rho} \quad (3.23)$$

The mixture is unpolarized when population difference  $\delta_\rho = 0$  and completely polarized when  $\delta_\rho = P$  in which case only one component exists.

This leads to

$$\frac{2p}{3} = \int x^2 dx [n(\hat{\omega}_1) - n(\hat{\omega}_2)] \quad (3.24)$$

Thus system is described by the universal dimensionless parameters: interaction strength or coupling constant,  $(k_F a)^{-1}$ , mass ratio  $q$ , polarization  $P$  measuring the population imbalance together with temperature  $T$  scaled with respect to Fermi temperature  $T_F$ . The three interaction regimes with  $(k_F a)^{-1}$  are:

- BCS regime  $(k_F a)^{-1} < -1$
- crossover regime :  $-1 \leq (k_F a)^{-1} \leq 1$
- BEC regime :  $(k_F a)^{-1} > 1$

### 3.3 Thermodynamic Potential

The evolution of BCS phase as a function of chemical potential difference  $h$  at zero-temperature (64) is shown in the Fig. 3.1. We consider the mass symmetric case here corresponding to  $q = 1$ . In this case  $\delta\xi = -h$ . The thermodynamic potential as a function of gap  $\Delta$  at different applied chemical potential difference  $h$  is studied. At  $h = 0$ , normal state corresponding to  $\Delta = 0$  is maximum and minimum is located at BCS order parameter,  $\Delta$ . As  $h$  is increased, at  $h = \Delta/2$  minimum develops at  $\Delta = 0$  which becomes degenerate with BCS minimum at critical value  $h_c = \Delta/\sqrt{2}$ . This critical value of  $h$  is called Clogston-Chandrasekhar limit. Beyond this critical point BCS state becomes unstable to normal state. However, there appears an

intermediate maximum which corresponds to the breached pair (BP) state.

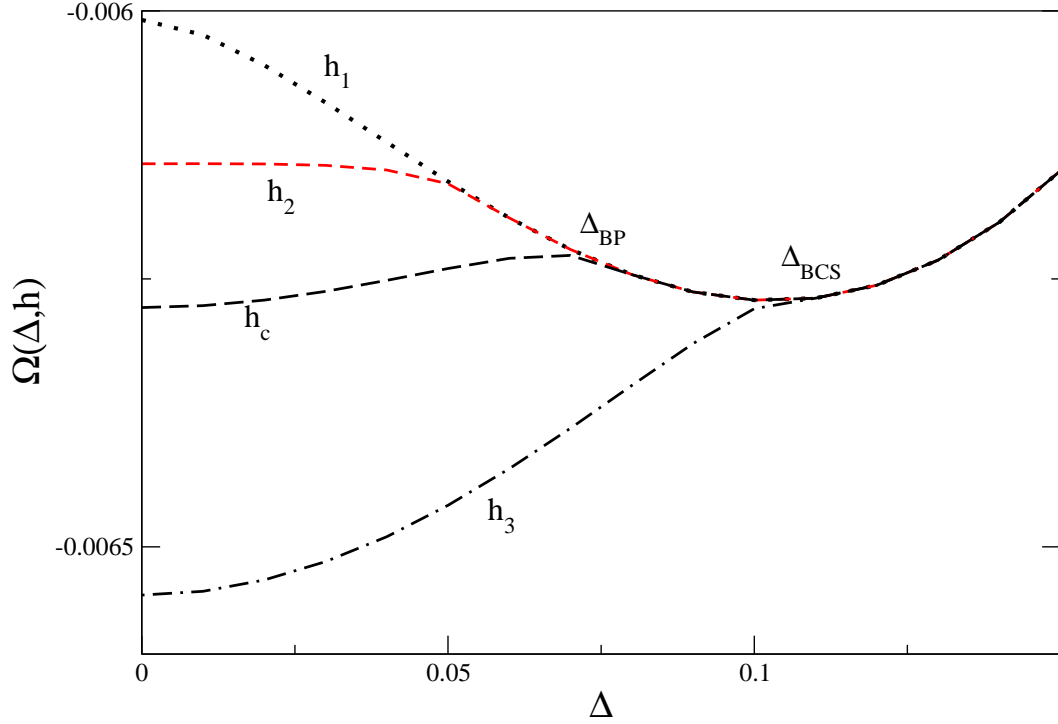


Fig. 3.1: The thermodynamic potential  $\Omega$  in units of  $E_F k_F^3$  for mass symmetric case at zero-temperature vs  $\Delta$  is plotted at  $(k_F a)^{-1} = -1$  at fixed chemical potential  $\mu = 0.48$  for various values of chemical potential difference  $h$ . At  $h_0 = 0$ , without chemical potential difference,  $\Omega$  has minimum at  $\Delta = \Delta_{\text{BCS}}$  corresponding to BCS superfluid. As  $h$  is increased, a local minimum appears at  $\Delta = 0$ . This local minimum becomes degenerate at  $h_c = \Delta/\sqrt{2}$ . Also, a local maximum develops at  $\Delta = \Delta_{\text{BP}}$ . For  $h > h_3 = \Delta$ , the BCS minimum disappears.

We have found that Clogston-Chandrasekhar limit  $h_c = \Delta/\sqrt{2}$  is accurate only in BCS regime of interaction and increases as unitarity is approached thus showing dependence on the coupling  $(k_F a)^{-1}$ . In fact we found it to be  $h_c = 1.44\Delta$  at unitarity in agreement with (38).

### 3.4 BCS-BEC Crossover

We first consider the crossover from a BCS state to a Bose-Einstein condensate (BEC) at  $T = 0$ . The system is characterized by equal masses and densities. There are two extremes of the crossover. BCS regime with weak attractive interactions, characterized by a small negative scattering length

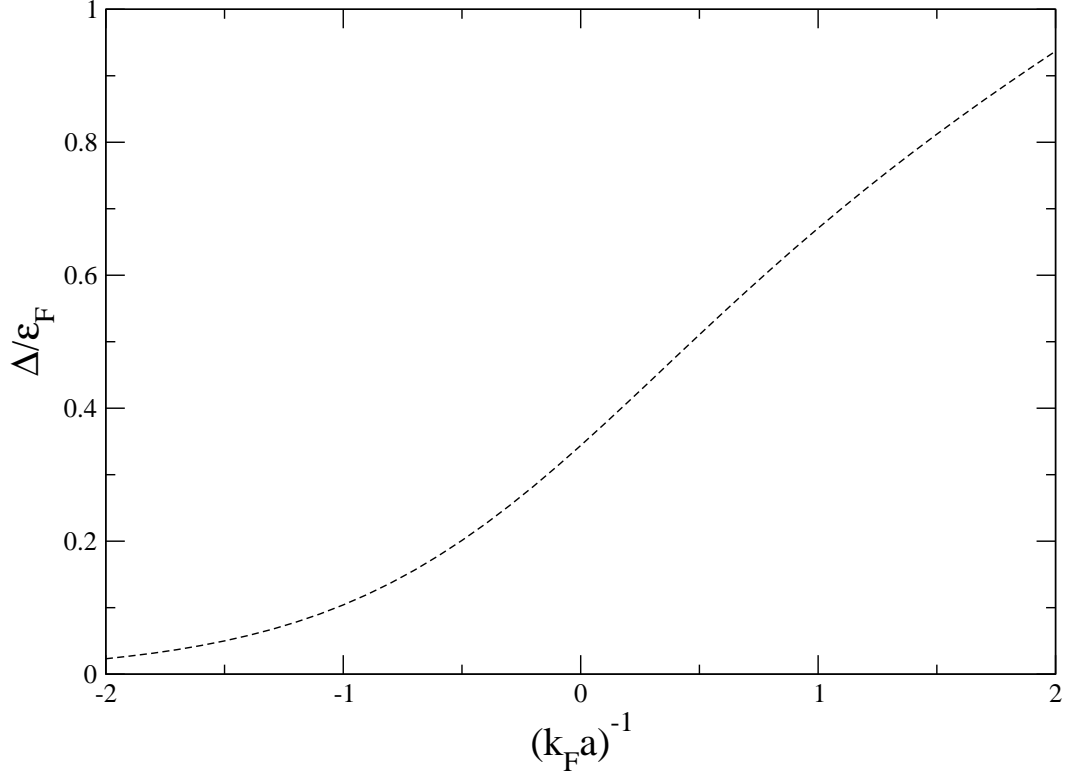


Fig. 3.2:  $\hat{\Delta}$  is plotted against coupling  $(k_F a)^{-1}$  at zero temperature without population imbalance.

$a$ , lead to collective Cooper pairing of atoms and BCS superfluidity. In the opposite limit of strong attraction, characterized by a small positive scattering length  $a$ , one obtains bosonic molecules which exhibit Bose-Einstein Condensation (BEC).

The first theoretical treatment of BCS to BEC crossover was given by Eagles in the context of superconductivity in systems with low carrier concentrations. Subsequently Leggett studied the dilute gas of fermions at  $T = 0$  using a variational approach based on BCS wave function. He showed that as the strength of the interaction is varied there was a smooth crossover from a BCS ground state with Cooper pairs overlapping in real space to tightly bound diatomic molecules.

In this case, gap and number density equation at  $T = 0$  respectively reads

$$-\frac{\pi}{k_F a} = \int_0^\infty x^2 dx \left[ \frac{1}{\hat{\omega}} - \frac{1}{\hat{\epsilon}} \right], \quad (3.25)$$

$$\frac{2}{3} = \int x^2 dx \left[ 1 - \frac{\hat{\xi}}{\hat{\omega}} \right] \quad (3.26)$$

The weak coupling case in the standard BCS theory, effect of interaction on the chemical potential is neglected by setting  $\nu \simeq E_F$ . To describe the crossover, the change in chemical potential due to interaction is incorporated. Hence the chemical potential  $\nu$  is determined self-consistently with the order parameter  $\Delta$ .

Fig. 3.2 shows the variation of  $\Delta$  with coupling  $(k_F a)^{-1}$ . In the BCS regime where  $(k_F a)^{-1} < -1$ ,  $\Delta$  is exponentially small in agreement with analytic solution as given in (7). The variation of chemical potential  $\nu$  is shown in the Fig. 3.3. The chemical potential  $\nu$  decreases as the coupling  $(k_F a)^{-1}$  increases and it is zero at  $(k_F a)^{-1} \approx 0.55$ . It is negative at higher values of  $(k_F a)^{-1}$ , which indicates the formation of Bose-Einstein condensation of diatomic molecules of fermionic atoms.

Let us consider the single Fermionic excitations  $\omega$  given by

$$\omega = \sqrt{(\epsilon_k - \nu)^2 + \Delta^2}. \quad (3.27)$$

If  $\nu > 0$  then minimum of  $\omega$  attains the value  $\Delta$ . This is related to pair dissociation energy. However, if  $\nu < 0$ , the minimum lies at  $\sqrt{\nu^2 + \Delta^2}$ . Thus, for  $\nu < 0$  which indicates formation of molecule, excitation energy is related to molecular binding energy.

At the unitary point,  $|a| \rightarrow \infty$  i.e.  $(k_F a)^{-1} = 0$ . It is interesting to note that in this limit, the scattering length is no longer a physical length scale, and that the only energy scale in the problem is that set by the density, i.e., the Fermi energy of the corresponding free gas,  $E_F$ .

As a result, thermodynamic quantities only depend on the Fermi energy  $E_F$ , such that we have  $\nu = (1 + \beta)E_F$  and where  $(1 + \beta)$  is dimensionless universal constant.

Quantum Monte Carlo (QMC) calculations (65; 66; 67) obtain  $(1 + \beta) =$

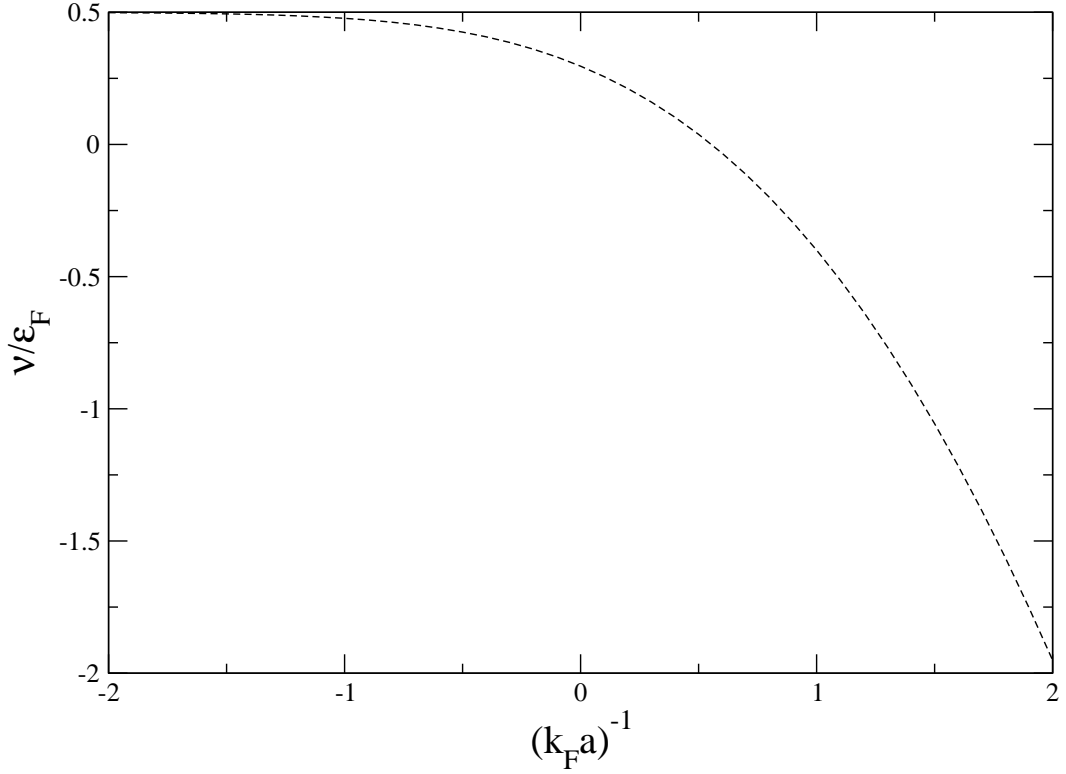


Fig. 3.3:  $\hat{\nu}$  is plotted against coupling  $(k_F a)^{-1}$  at zero temperature without population imbalance.

0.44, while experiments (68; 17; 69; 16) find  $(1+\beta)$  in the range 0.32 to 0.44. In contrast, mean field (MF) theory yields  $(1+\beta) = 0.59$  and  $\Delta = 0.68\nu$ . Thus in the strong coupling case order parameter or pairing gap is of the order of Fermi energy  $E_F$  rather than exponentially suppressed as in the weak coupling BCS regime.

### 3.5 Breached Pair solution

Consider the system with mismatched Fermi momenta. This can occur when there is a difference between the densities or a difference in the masses of the two fermion species. In this case quasiparticle energies have two branches

$$\omega_{1,2} = \omega \pm \delta_\xi. \quad (3.28)$$

Without loss of generality, one can choose  $\delta_\xi < 0$ . In this case  $\Theta(-\omega_2) = 0$  as  $\omega_2 > 0$  always. This convention, that is,  $\delta_\xi < 0$  physically means that component with mass  $m_1$  are in majority. This is easily seen for systems with the same mass. Here  $\delta_\xi = -\delta_\nu$  and  $\delta_\xi < 0$  means  $\delta_\nu > 0$ . This naturally leads us to the result that component with mass  $m_1$  are in majority. Now  $\Theta(-\omega_1)$  where  $\omega_1 = \omega + \delta_\xi$  contribute only when  $\omega_1 < 0$ .

The momenta at which  $\omega_1 = 0$  correspond to gapless modes. This change from gapped to gapless modes gives rise to change in density distribution also. These points at which  $\omega_1 = 0$ , are given by

$$\begin{aligned} \hbar^2 k_{\max/\min}^2 &= (m_1 \nu_1 + m_2 \nu_2) \\ &\pm \sqrt{(m_1 \nu_1 - m_2 \nu_2)^2 - 4m_1 m_2 \Delta^2}. \end{aligned} \quad (3.29)$$

The breached pair state is characterized by number of zeroes in  $\omega_1$ . This corresponds to zero energy surface in the momentum space. If  $\omega_1$  support two zeros it is called breached pair state with two Fermi surface (BP2). This phase is also referred to as *interior gap* phase (23). Similarly, if  $\omega_1$  support one zero then it is breached pair state with one Fermi surface (BP1) (70). Let us recall that normal matter excitation energies vanish at the Fermi surface. Notice that the Fermi sea for the excess fermion is spherical shell in  $k_{\min} \leq k \leq k_{\max}$  for BP2 state and sphere with radius  $0 \leq k \leq k_{\max}$ . It should be noted that when  $\delta_\xi = 0$ , that is when there is no mismatch in Fermi momenta, step functions  $\Theta(\dots)$  don't contribute as  $\omega \geq 0$ . This situation corresponds to standard BCS case where Fermi momenta are equal.

Next we present the gap, number density equations and thermodynamic potential. In our convention  $\delta_\xi \leq 0$  corresponding to the situation where component with mass  $m_1$  are in majority. In this case

$$\Theta(-\omega_1) = 1 \quad \text{for} \quad k_{\min} \leq k \leq k_{\max}, \quad (3.30)$$

$$\Theta(-\omega_2) = 0 \quad (3.31)$$

This leads to the following set of equations: Gap equation

$$-\frac{\pi}{k_F a} = \int_0^\infty \frac{x^2 dx}{\hat{\omega}} \left[ 1 - \Theta(-\hat{\omega}_1) \right] - \frac{1}{\hat{\varepsilon}}, \quad (3.32)$$

the total density equation,

$$\frac{2}{3} = \int x^2 dx \left[ 1 - \frac{\xi}{\omega} (1 - \Theta(-\hat{\omega}_1)) \right], \quad (3.33)$$

polarization equation

$$\frac{2p}{3} = \int x^2 dx [\Theta(-\hat{\omega}_1)] \quad (3.34)$$

$$= \frac{1}{3} \left( \hat{k}_{\max}^3 - \hat{k}_{\min}^3 \right) \quad (3.35)$$

thermodynamic potential density

$$\hat{\Omega} = \frac{1}{2\pi^2} \int x^2 dx \left[ \hat{\xi} - \hat{\omega} + \hat{\omega}_1 \Theta(-\hat{\omega}_1) \right] - \frac{\hat{\Delta}^2}{\hat{g}}. \quad (3.36)$$

### 3.6 Results and Discussions

Let us note that the dimensionless parameters which describe the Fermionic mixture are the dimensionless coupling  $(k_F a)^{-1}$ , polarization  $P$ , temperature  $T$  in units of  $T_F$  and mass ratio  $q$ . The gap equation, Eq. (4.15), together with the number density equations, that is, the average density given by Eq. (3.22) and polarization given by Eq. (3.24), are solved self consistently to obtain order parameter  $\hat{\Delta}$ , and chemical potentials  $\hat{\nu}$  and  $\hat{\delta}_\nu$ . The thermodynamic potential difference is then calculated using these parameters.

Now we consider the case of nonzero polarization, however, for symmetric mass case, i.e., with  $m_1 = m_2$ . In such a case, the breached pair phase shall have Fermionic gapless modes. The gapless modes occur when  $\omega_i = 0$ . Without loss of generality, we shall assume here  $\delta_\xi$  as negative. For mass symmetric case,  $q = 1$  and hence  $\delta_\xi = -\delta_\nu$ . In this case

only  $\omega_1$  can become zero. Thus gapless mode means  $\omega = |\delta_\xi|$ . Depending on the chemical potentials, breached pair solution can exist either with one ( $\nu_2 < 0$ ) or two ( $\nu_1, \nu_2 > 0$ ) Fermi surfaces referred to as BP1 and BP2 phase respectively (23; 70).

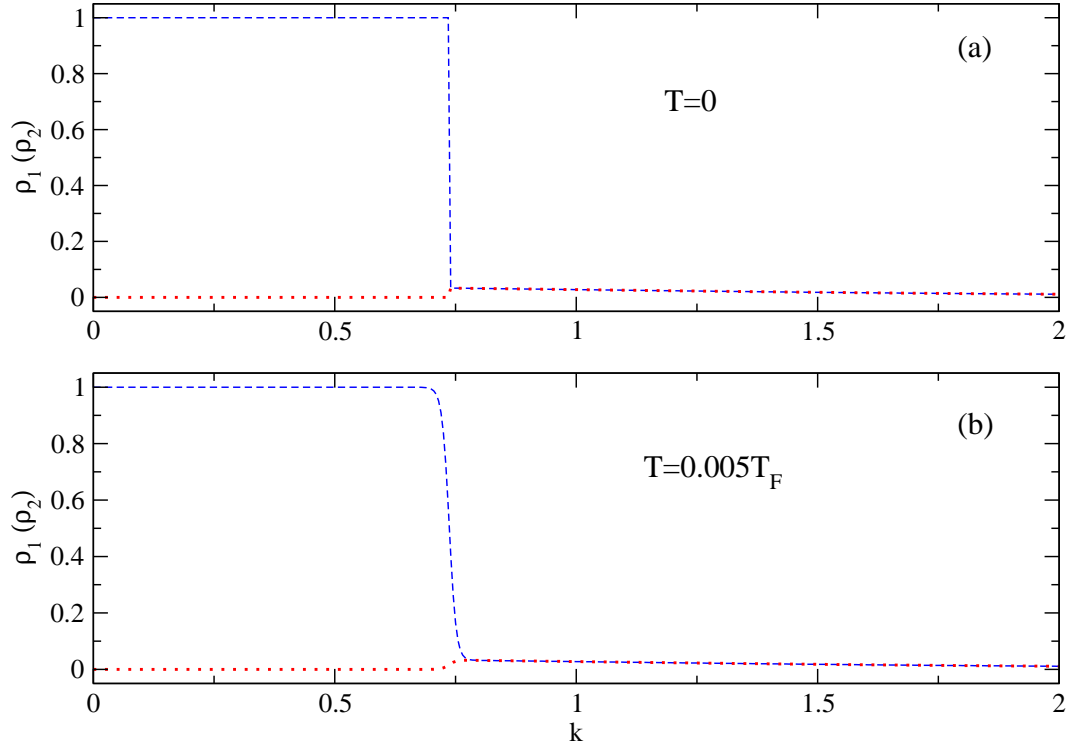


Fig. 3.4: The momentum space density profile for mass symmetric case  $q = 1$  at (a)  $T = 0$  (b)  $T = 0.005T_F$ . Here  $(k_F a)^{-1} = 2$  and  $P = 0.2$ . The profile corresponds to BP1 phase.

We find that breached pair phase with one Fermi surface (BP1) starts to become stable for couplings  $(k_F a)^{-1} > 1$ . The Fig. 3.4 shows the density profile for mass symmetric case at zero and finite temperatures in the BEC regime of interaction. The density profile here corresponds to  $(k_F a)^{-1} = 2$  and  $P = 0.2$  and has the characteristic of BP1 phase of a single Fermi surface. We also verify here that the thermodynamic potential difference between the paired phase and the normal matter is negative indicating its stability. The critical polarization  $P_c$  up to which this phase is stable for this coupling is  $P_c = 0.52$ . As the coupling increases, the critical polarization  $P_c$  increases and finally reaches  $P_c = 1$  at  $(k_F a)^{-1} \approx 2.3$ . The upper and

lower curves correspond to zero temperature and  $T/T_F = 0.005$ . Finite temperature effects smoothen the distribution functions.

We also observe that, at unitarity ( $(k_F a)^{-1} = 0$ ), breached pair solution exists with two Fermi surfaces (BP2). However it is thermodynamically unstable i.e.  $\delta\Omega$  is positive. The density profile in momentum space is shown in the Fig. 3.5. We have also shown the effect of temperature in the density profiles within the present mean field calculation. As before, the density profiles get smoothened for finite temperatures as quasi-particle density distribution is no longer a  $\Theta(\dots)$  function.

Thus, with population imbalanced equal mass case, the breached pair with one Fermi surface (BP1) is stable in the BEC regime of interaction. However, in presence of mass asymmetry, i.e., when two components have unequal masses, the system is proposed (71) to support breached pairing with two Fermi surfaces (BP2).

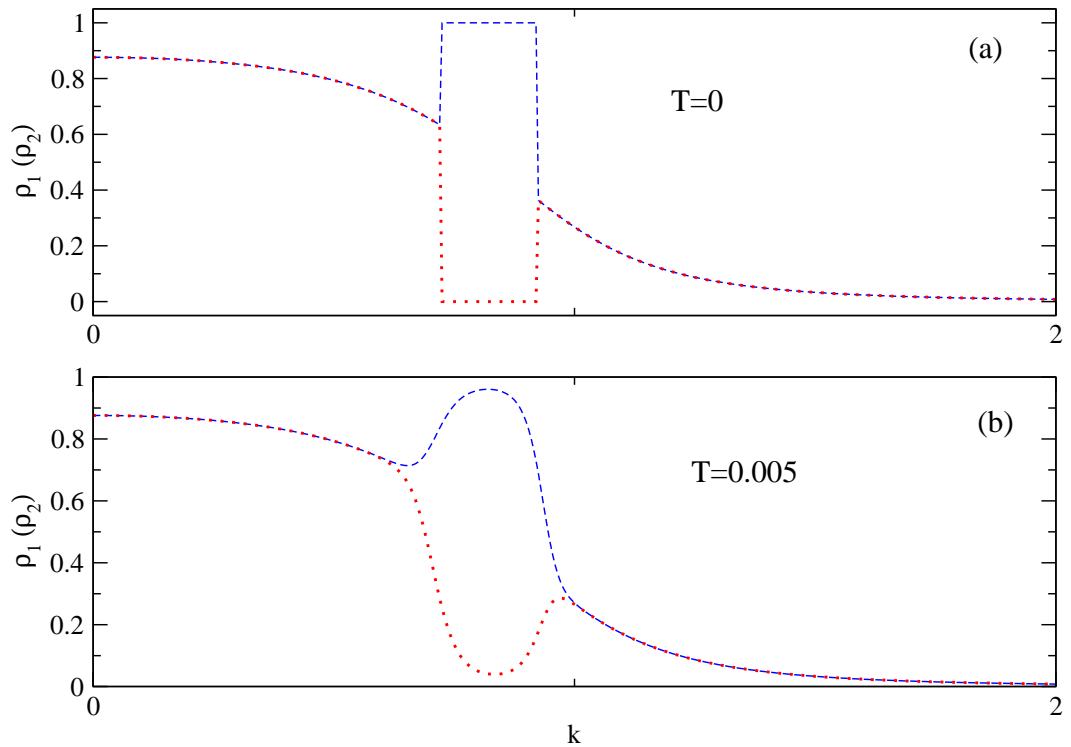


Fig. 3.5: The momentum space density profile for mass symmetric case  $q = 1$  at (a)  $T = 0$  (b)  $T = 0.005T_F$ . Here  $(k_F a)^{-1} = 0$  and  $P = 0.2$ . The profile corresponds to BP2 phase. This phase, however, is unstable.

To explore this situation, we next consider the mass asymmetric case with the mass ratio  $q = m_1/m_2$  differing from unity. Specifically, we have taken the mass ratio  $q = 0.15$ . This ratio corresponds to  ${}^6\text{Li}$ - ${}^{40}\text{K}$  mixture, which has been cooled to degeneracy recently (52; 53), with  ${}^6\text{Li}$  chosen as the majority population. The momentum space density profile for this system at  $(k_F a)^{-1} = 0.1$  and  $P = 0.2$  is shown in the Fig. 3.7. Though the coupling strength is close to unitarity, the phase corresponds to the gapless modes with one Fermi surface (BP1). The critical polarization turns out to be  $P_c \approx 0.35$ . If we consider  ${}^{40}\text{K}$  as majority component, the breached pairing

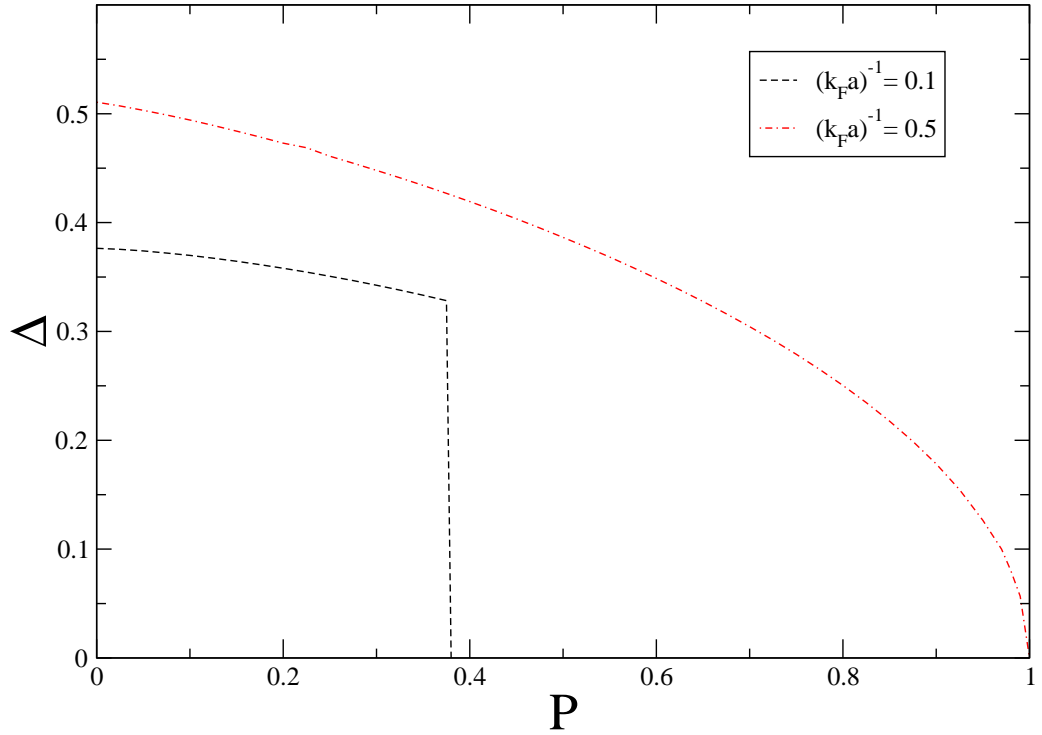


Fig. 3.6: The variation of  $\Delta$  against polarization is shown for  $m_1/m_2 = 0.15$  at couplings  $(k_F a)^{-1} = 0.1$  (dashed) and  $(k_F a)^{-1} = 0.5$  (dot-dashed).

solution with one Fermi surface exists in the deep BEC regime. For example for  $(k_F a)^{-1} = 8$ , we find the stable BP1 state up to the critical polarization  $P_c \approx 0.22$ .

This trend is found to be common to other mass ratios. We have taken other values of mass ratios and found that breached pairing with two Fermi surfaces is never stable phase. Thus breached pairing with one Fermi sur-

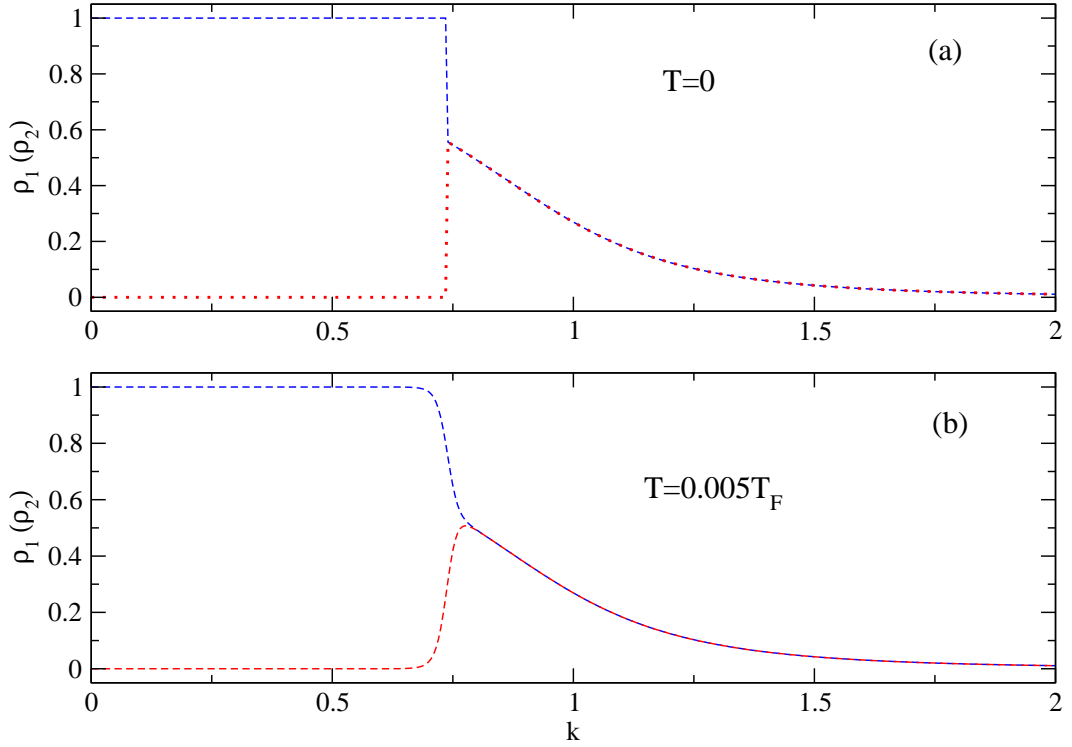


Fig. 3.7: The momentum space density profile for mass asymmetric case  $q = 0.15$  at (a)  $T = 0$  (b)  $T = 0.005T_F$ . Here  $q = m_1/m_2$ ,  $(k_F a)^{-1} = 0.1$  and  $P = 0.2$ . The profile corresponds to BP2 phase. This is stable phase.

face (BP1) is only stable phase. The threshold of stability, i.e., the minimum interaction strength for BP1 state to be stable, however, can be varied by changing the mass ratios. With lighter atoms as the majority component, this threshold decreases whereas with heavier atoms forming the majority component, it increases further deep into the BEC regime of interaction.

### 3.7 Summary

In this chapter, we have studied BCS-BEC crossover and compared the results with Monte Carlo calculations and experiments. It is found that mean field calculation overestimates the universal constant  $(1 + \beta)$ . We have also found that Clogston-Chandrasekhar limit, beyond which BCS state becomes unstable to normal state, increases as the unitarity is approached. In contrast to its value  $h_c = \frac{\Delta}{\sqrt{2}}$  in BCS regime, it becomes  $h_c = 1.44\Delta$  at unitarity.

We discuss the gapless *breached pairing* phase which has two possible states: breached pair with one Fermi surface (BP1) and breached pair with two Fermi surfaces (BP2). We obtain the important result that breached pairing with one Fermi surface (BP1) is only ever stable ruling out the proposal that in presence of mass asymmetry, breached pair with two Fermi surface (BP2) may become stable.

For equal mass case, breached pair with one Fermi surface (BP1) is stable only in the BEC regime. However, in presence of mass asymmetry the threshold of stability can be affected. In particular,  ${}^6\text{Li}$ - ${}^{40}\text{K}$ , mixture relevant for present experimental efforts studied. With light atoms forming the majority component, this threshold decreases and shifts towards unitarity. In contrast, with heavier atoms as the majority, it further shifts into the BEC regime.

## Chapter 4

# Trapped Systems

We have thus far studied homogeneous or bulk system. The atomic-gas experiments are performed in the trap. Thus to make connection with the experiments trap effect has to be included. We consider the equal mass case and to avoid notational confusion we represent quasiparticle energies  $\omega_i$  as  $E_\sigma$  where now  $\sigma = \uparrow, \downarrow$  represent two pseudo spin (hyperfine) states. Furthermore we use  $\omega_\sigma$  to represent trap frequencies.

In particular we consider the trap imbalanced system where each component experiences different trapping potential ( $\omega_\uparrow \neq \omega_\downarrow$ ). The trap imbalanced is naturally realized with Fermi mixture with unequal masses where each component experiences different potential due to the mass difference. The ground state properties for this system have been studied in (72; 54; 73; 74). However, it was recently proposed in (75) that even equal mass Fermi mixture can admit trap imbalance and the system was studied with population balance (75) and small trap imbalance (55). It is proposed, for example, in the case of magnetically trapped systems (the system we consider here), trapping two hyperfine states of a particular atom which have different magnetic moments corresponds to a situation where  $m_\uparrow = m_\downarrow$  and  $\omega_\uparrow \neq \omega_\downarrow$ .

We include the trap effect via local density approximation. The system we consider is a trapped cloud of two-component Fermionic mixture confined by harmonic isotropic potential  $V_{T\sigma}(r)$  where  $r$  measures the distance

from the trap center.

Before presenting the method we must construct the phase diagram where each point in the trap is represented by the corresponding value for the coordinate  $(\mu(r), h(r))$  where  $\mu(r)$  and  $h(r)$  are respectively the average and difference local chemical potentials. This is achieved in Sec. 4.1. The method to include trap under local density approximation is introduced in Sec. 4.2 which is then generalized to imbalanced trap case where each component of the Fermi mixture experiences different trap frequency from the other. The effects of this trap imbalance are discussed in Sec. 4.3. The results are summarized in Sec. 4.4

## 4.1 Phase Diagram

Now we construct the zero temperature phase diagram in grand canonical ensemble (64) of fixed  $\mu$  and  $h$ .

We start with  $h = 0$  and using the gap equation find the point where the superfluid state makes a continuous transition to the vacuum state of molecules. This value of  $\mu$  is denoted by  $\mu_c$ . For small  $h < h_m$  this behavior i.e. superfluid-to-vacuum, persists and leads to a vertical phase boundary in the phase diagram Fig. 4.1. It should be noted that  $h_m$  represent the chemical potential difference beyond which system starts to admit population imbalance. The gap equation is given by

$$-\frac{\tilde{m}}{2\pi\hbar^2 a} = \frac{1}{(2\pi)^3} \int d^3k \left[ \frac{1}{2E} (1 - \Theta(-E_\uparrow) - \Theta(-E_\downarrow)) - \frac{1}{2\varepsilon_k} \right]. \quad (4.1)$$

Next, we start with  $\mu < \mu_c$  and increasing  $h$ . Here the system evolve from vacuum state to polarized normal state as  $\mu_\uparrow = \mu + h$  is now positive quantity leading to finite population of the  $\uparrow$ -fermions. There cannot be a superfluid phase here as  $\mu < \mu_c$ . This leads to the vacuum-to-polarized normal N

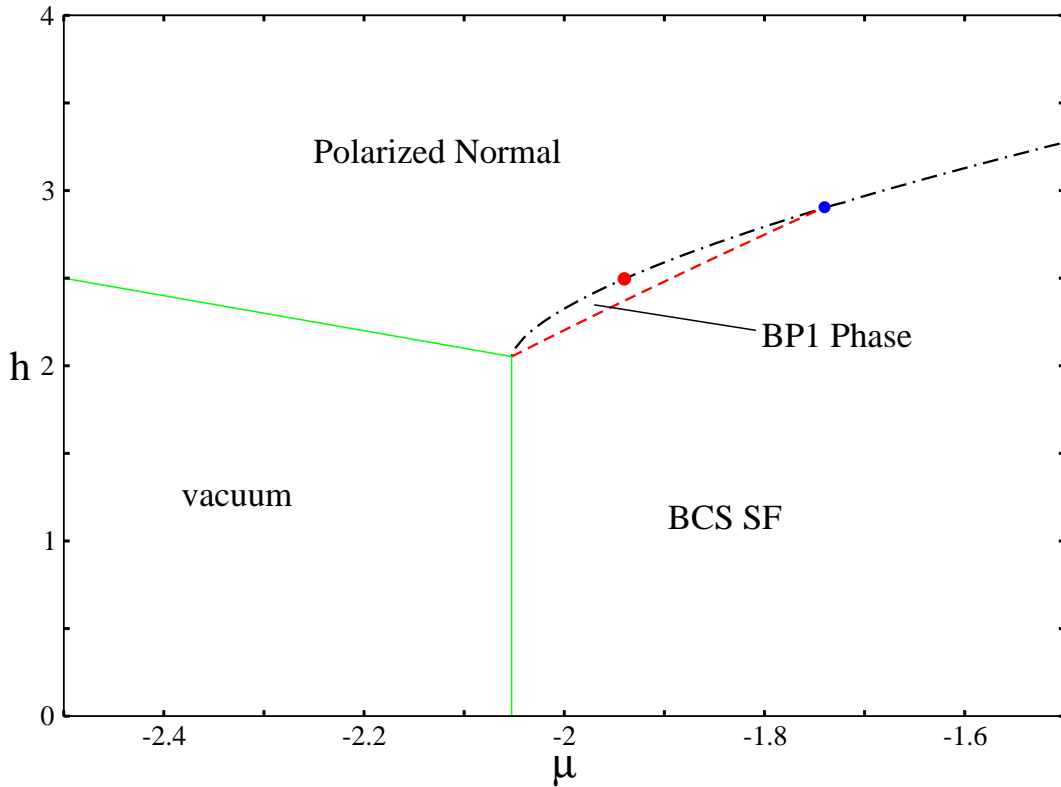


Fig. 4.1: The zero temperature phase diagram for  $(k_F a)^{-1} = 2.0$  showing unpolarized superfluid (BCS SF), polarized superfluid (BP1), vacuum, and polarized normal (N) phases. The upper (blue) dot denotes the point beyond which the BP1 state ceases to exist. The lower (red) dot represents the tricritical point. The dashed (red) line indicates the second-order transition between the unpolarized SF and BP1 phase. The dot-dashed (black) line indicates the first-order transition between the SF to polarized N state and the BP1 to normal above and below the upper (blue) point, respectively.

phase boundary.

Similarly we start with  $\mu > \mu_c$  with increasing  $h$ . Here the system makes a continuous transition to breached pair state as superfluid starts to admit finite polarization. The superfluid-to-BP1 boundary is calculated by numerical comparison of the thermodynamic potentials in the respective states. As we further increase the  $h$ , the BP1 eventually makes transition to polarized normal state. However, depending on the value of  $\mu$  the BP1-to-polarized normal transition can be first or second order. The tricritical point where first and second order transition meet is indicated in the phase diagram as red dot. Also the BP1-Normal first order curve intersects the superfluid-BP1 curve at large  $\mu$ . Beyond this intersection point, BP1 ceases to exist and there is direct first order superfluid to normal state transition. This completes the construction of the phase diagram. We next consider the trapped Fermions in isotropic harmonic potential.

## 4.2 Trapped Fermions

We have thus far studied homogeneous or bulk system. The atomic-gas experiments are performed in the trap. Thus to make connection with the experiment trap effect has to be included. The trap potential in experiments are harmonic and varies smoothly on the scale of Fermi wavelength. For simplicity we choose isotropic harmonic trap.

$$V_T(r) = \frac{1}{2}m\omega_T^2 r^2 \quad (4.2)$$

In this situation trap potential is included as local density approximation (LDA) approximating the system as locally uniform with local chemical potential. This semi-classical approximation, assume the properties of the gas at point  $\mathbf{r}$  to be those of uniform gas having a density equal to the local density  $\rho(\mathbf{r})$ . It is valid when Fermi energy is much larger than the trap level

spacing. This condition is met by the current atomic gas experiments. Thus, the local chemical potential is given by

$$\mu(r) = \mu - V_T(r),$$

where  $\mu$  is the chemical potential enforcing total number of particle constraint. The chemical potentials of each component at a given point in the trap are given by

$$\mu_{\uparrow}(r) = \mu(r) + h, \quad (4.3)$$

$$\mu_{\downarrow}(r) = \mu(r) - h, \quad (4.4)$$

where  $h$  is chemical potential difference which remain uniform if the two components experience the same trapping potential. The quantities  $\mu$  and  $h$  are determined by enforcing particle number constraints namely total number of atoms and polarization respectively.

We consider the system where each component experience different trapping potential  $V_{T\sigma}$ . In this case  $h$  is no longer uniform and varies with position in space. The local chemical potential for each component at any point in the trap can be written as

$$\mu_{\uparrow}(r) = \mu(r) + h(r), \quad (4.5)$$

$$\mu_{\downarrow}(r) = \mu(r) - h(r), \quad (4.6)$$

where

$$\mu(r) = \mu - V_T(r), \quad (4.7)$$

$$h(r) = h - \delta V_T(r), \quad (4.8)$$

and

$$V_T(r) = \frac{V_{T\uparrow} + V_{T\downarrow}}{2}, \quad (4.9)$$

$$\delta V_T(r) = \frac{V_{T\uparrow} - V_{T\downarrow}}{2}. \quad (4.10)$$

In terms of  $n(r) = n_\uparrow(r) + n_\downarrow(r)$  and  $m(r) = n_\uparrow(r) - n_\downarrow(r)$ , the total number of atoms  $N$  and population imbalance  $\Delta N$  are given by

$$N = \int d^3r n(r), \quad (4.11)$$

$$\Delta N = \int d^3r m(r), \quad (4.12)$$

where

$$\begin{aligned} n_\uparrow(r) &= \frac{1}{(2\pi)^3} \int d^3k \left[ \frac{1}{2} \left( 1 + \frac{\xi(r)}{E(r)} \right) \Theta(-E_\uparrow(r)) \right. \\ &\quad \left. + \frac{1}{2} \left( 1 - \frac{\xi(r)}{E(r)} \right) (1 - \Theta(-E_\downarrow(r))) \right] \end{aligned} \quad (4.13)$$

$$\begin{aligned} n_\downarrow(r) &= \frac{1}{(2\pi)^3} \int d^3k \left[ \frac{1}{2} \left( 1 + \frac{\xi(r)}{E(r)} \right) \Theta(-E_\downarrow(r)) \right. \\ &\quad \left. + \frac{1}{2} \left( 1 - \frac{\xi(r)}{E(r)} \right) (1 - \Theta(-E_\uparrow(r))) \right], \end{aligned} \quad (4.14)$$

where  $\Theta(\dots)$  is the Heaviside step function, the zero-temperature limit for Fermi-Dirac distribution. The local gap equation is

$$-\frac{\tilde{m}}{2\pi\hbar^2 a} = \frac{1}{(2\pi)^3} \int d^3k \left[ \frac{1}{2E(r)} (1 - \Theta(-E_\uparrow(r)) - \Theta(-E_\downarrow(r))) - \frac{1}{2\varepsilon_k} \right]. \quad (4.15)$$

The trap introduces the new length scale called Thomas-Fermi radius defined as

$$R_{TF} = \sqrt{\frac{2\mu}{m\omega_T^2}}. \quad (4.16)$$

Note further that in the BEC regime, chemical potential  $\mu$  is already negative at the center of the trap and hence  $\mu(r)$  does not vanish. We also note that in the deep BEC regime  $\mu = -E_b/2$  (63) where the molecular binding energy

$E_b = 1/2\tilde{m}a^2$ . Thus we impose the condition (64),

$$\mu(R_{TF0}) = \mu_0 - \frac{1}{2}m\omega_T^2 R_{TF0}^2 = -\frac{E_b}{2}. \quad (4.17)$$

This gives,

$$R_{TF0} = \sqrt{\frac{E_b(2\mu_0 + 1)}{m\Omega_T^2}}. \quad (4.18)$$

The zero subscript indicates that the quantities are for zero polarization. To investigate the system numerically we define the dimensionless quantities  $\hat{\Delta}(r) = \Delta/E_F$ ,  $\hat{\mu}(r) = \mu(r)/E_F$ ,  $\hat{h}(r) = h(r)/E_F$  where we choose  $E_F = (6N)^{1/3}\hbar\omega_T$  with  $\omega_T = \sqrt{\omega_\uparrow^2 + \omega_\downarrow^2}$ . We also normalize the distance in the trap  $x = r/R_{TF0}$  and define  $k_F$  by the relation  $E_F = \hbar^2 k_F^2 / 2\tilde{m}$ . Hence

$$\hat{\mu}_0(x) = \hat{\mu}_0 - x^2 \left( \hat{\mu}_0 + \frac{1}{(k_F a)^2} \right), \quad (4.19)$$

where we have expressed the binding energy  $E_b$  in  $E_F$  units as  $E_b = E_F / (k_F a)^2$ . However for the system with population imbalance we have

$$\begin{aligned} \hat{\mu}(x) &= \hat{\mu} - \left( \hat{\mu}_0 + \frac{1}{(k_F a)^2} \right) x^2, \\ \hat{h}(x) &= \hat{h} - \eta \left( \hat{\mu}_0 + \frac{1}{(k_F a)^2} \right) x^2, \end{aligned} \quad (4.20)$$

where dimensionless quantity

$$\eta = \frac{\omega_\uparrow^2 - \omega_\downarrow^2}{\omega_\uparrow^2 + \omega_\downarrow^2} \quad (4.21)$$

controls the trap asymmetry of the Fermi gas.

Next we consider the equation for total number of atoms and express it in normalized or dimensionless form appropriate for numerical investigation. The equations are  $N = \int d^3r n(r)$  and  $\Delta N = \int d^3r m(r)$  with  $n(r)$  and  $m(r)$  to be expressed in  $k_F^3$  and  $r$  in  $R_{TF0}$ . This normalization leaves us with factor

$k_F^3 R_{TF0}^3$ . By evaluating this factor, one obtains,

$$k_F^3 R_{TF0}^3 = 48N \left( \hat{\mu}_0 + \frac{\hat{E}_b}{2} \right)^{3/2} \quad (4.22)$$

Putting this into the equations, we get

$$\frac{1}{48} = 4\pi \left( \hat{\mu}_0 + \frac{\hat{E}_b}{2} \right)^{3/2} \int x^2 dx \hat{n}(\hat{\mu}(x), \hat{h}(x)), \quad (4.23)$$

$$\frac{p}{48} = 4\pi \left( \hat{\mu}_0 + \frac{\hat{E}_b}{2} \right)^{3/2} \int x^2 dx \hat{m}(\hat{\mu}(x), \hat{h}(x)). \quad (4.24)$$

The system for a given coupling strength and polarization  $P = \Delta N/N$  is investigated numerically in the following manner: first  $\mu_0$  is calculated by setting  $P = 0$ . Using Eq. (4.20) together with number and population imbalance equation,  $\mu$  and  $h$  are then calculated. It should be noted that in the deep BEC regime BP1 phase can be understood as mixture of composite bosons and fermion quasiparticles (51). In the BEC limit the order parameter ( $\Delta$ ) and density for composite bosons or molecular density are related (63; 64) via

$$n_m = \frac{\sqrt{2}c\pi}{4\sqrt{E_b}} \Delta^2 \quad (4.25)$$

with  $c = \frac{m^{3/2}}{\sqrt{3}\pi^2}$ . By calculating the local composite boson density ( $n_m$ ) and the magnetization ( $m$ ), the various phases are identified.

### 4.3 Results and Discussions

We choose experimentally accessible  $(k_F a)^{-1} = 2.0$  for the interaction strength. The phase at each spatial point of the trap is determined by the local chemical potentials  $\mu(r)$  and  $h(r)$  [see Eq. (4.20)] mapping it to the corresponding point in the phase diagram. As radius is increased  $(\mu(r), h(r))$  moves towards left in the phase diagram forming a line segment.

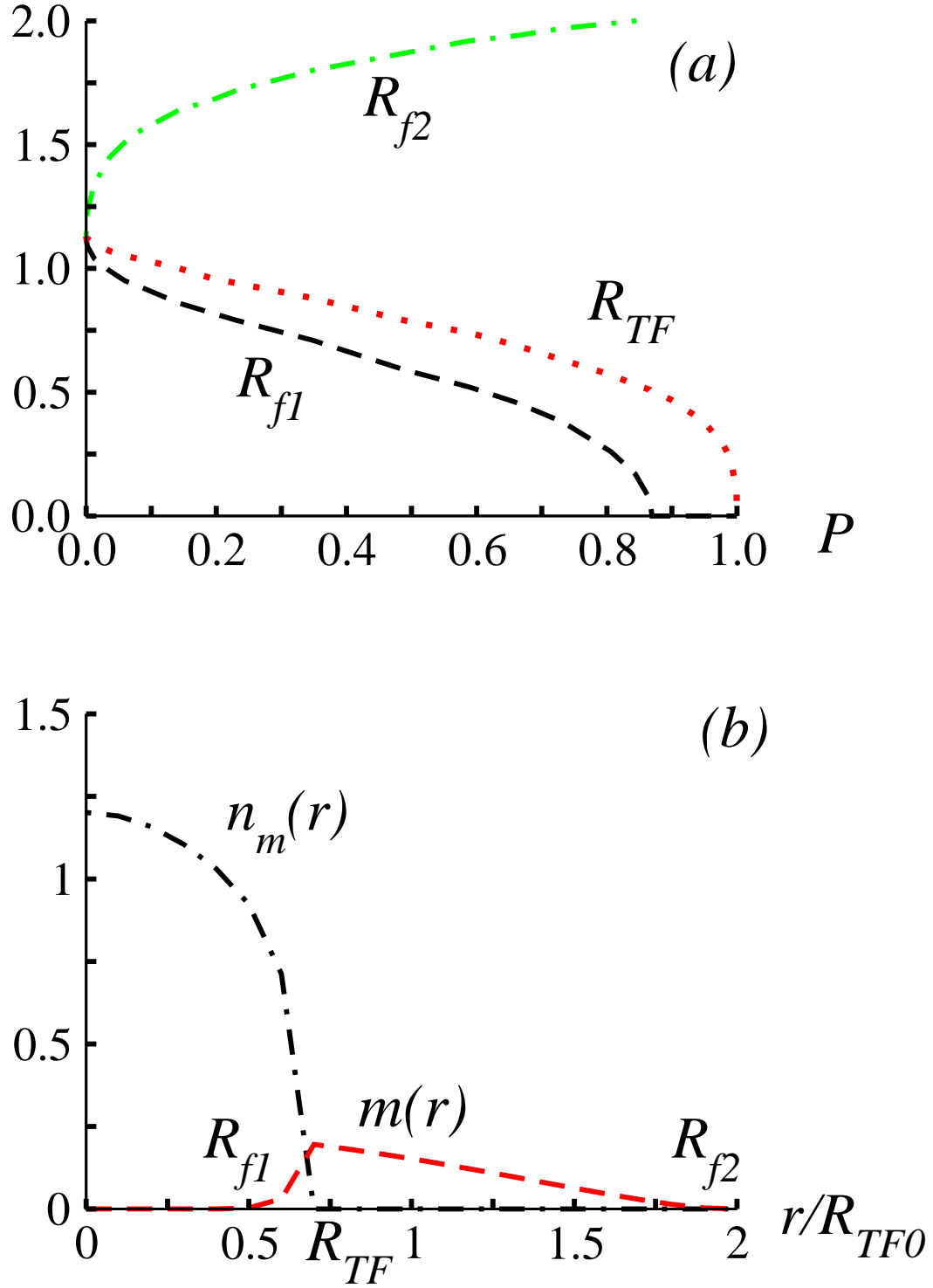


Fig. 4.2: (a) The three radii  $R_{f1}$  (outer boundary of unpolarized superfluid),  $R_{TF}$  (outer boundary of BP1 phase) and  $R_{f2}$  (outer boundary of N phase) plotted as a function of polarization  $P$  at trap asymmetry parameter  $\eta = 0$  and  $(k_F a)^{-1} = 2.0$ . (b) The molecular density  $n_m$  and magnetization  $m$  plotted against radius  $r$  measured in units of  $k_F^3$  and  $R_{TF0}$  respectively.

We find three different phases in the cloud. At the center, superfluid core where the population of the two components are equal, i.e., unpolarized superfluid (BCS SF), then an intermediate gapless superfluid, breached pairing with one Fermi surface (BP1) shell where fermion quasiparticles and composite bosons coexist and finally outer rim of normal majority component. This leads to three radii characterizing the shell structure:

- $R_{f1}$  where  $n_m \neq 0$  and  $m(r) = 0$  forming boundary for BCS SF phase. The quantity  $\Delta^2$  measures composite boson density and  $m(r)$  indicates the local polarization or population imbalance. For the BCS superfluid  $m(r) = 0$ . This defines the size of the unpolarized BCS superfluid.
- $R_{TF}$  above which  $n_m = 0$ . This indicates vanishing of order parameter and hence superfluidity. This defines the size of the superfluid core. The region  $R_{f1} < r < R_{TF}$  where  $n_m \neq 0$  and  $m(r) \neq 0$ , is composed of the polarized(gapless) superfluid (BP1).
- $R_{f2}$  above which  $m(r) = 0$ . Beyond this distance, no atoms exist and hence it demarcates the system measuring overall size of the system.

The three radii for the system without trap asymmetry  $\eta = 0$  as a function of polarization  $P$  together with density profiles showing  $n_m(r)$  and  $m(r)$  are shown in Fig. 4.2. The shell structure consist of BCS SF phase for  $r < R_{f1}$ , BP1 phase for  $R_{f1} < r < R_{TF}$  and finally polarized normal (N) state for  $R_{TF} < r < R_{f2}$ .

We next consider the system with trap asymmetry characterized by the dimensionless parameter  $\eta = (\omega_{\uparrow}^2 - \omega_{\downarrow}^2)/(\omega_{\uparrow}^2 + \omega_{\downarrow}^2)$ . The positive (negative)  $\eta$  value indicates that majority (minority) component is more tightly confined harmonically than the minority (majority) component. The three radii with different trap asymmetry parameter  $\eta$  as functions of polarization  $P$  are shown in Fig. 4.3. The value  $\eta = \pm 0.9$  corresponds to the situation when one of the component is very strongly confined. We start with  $\eta = -0.9$  corresponding to  $\omega_{\uparrow} \ll \omega_{\downarrow}$ . The BP1 shell here is very narrow and overall size

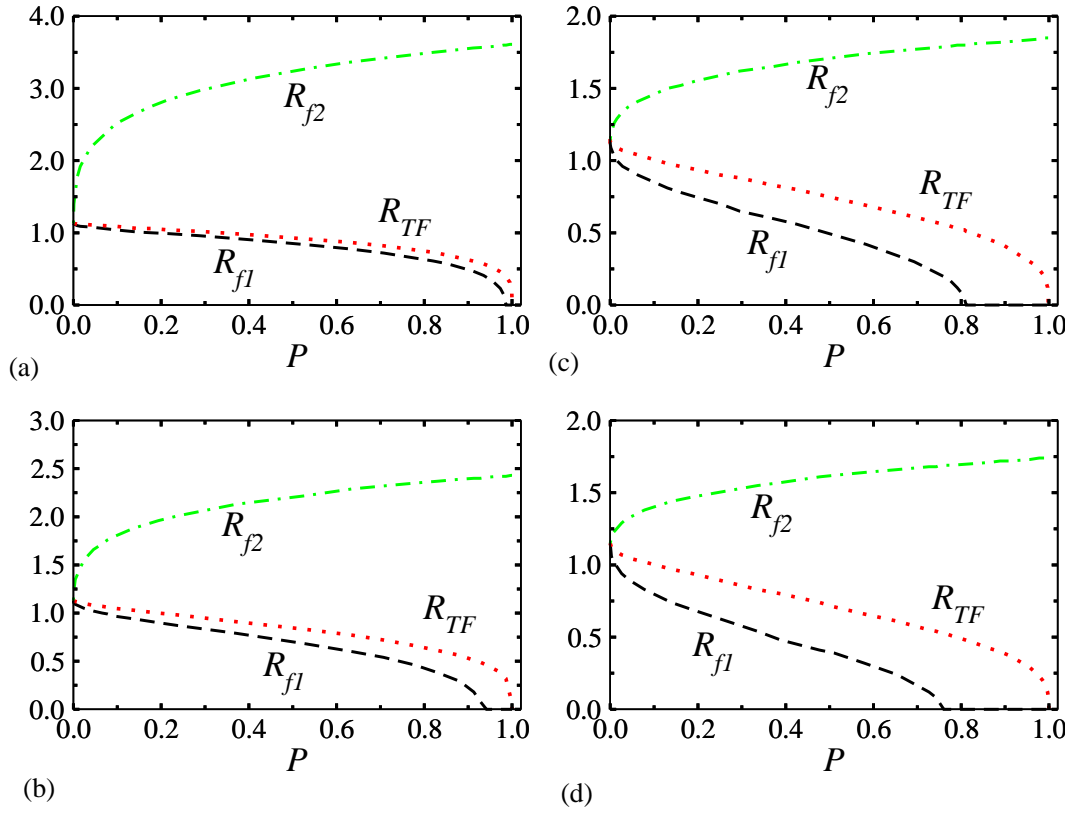


Fig. 4.3: The three radii  $R_{f1}$  (outer boundary of unpolarized superfluid),  $R_{TF}$  (outer boundary of BP1 phase) and  $R_{f2}$  (outer boundary of N phase) plotted as a function of polarization  $P$  for various values of the trap asymmetry parameter  $\eta$ . (a)  $\eta = -0.9$ , (b)  $\eta = -0.5$  (c)  $\eta = 0.5$ , (d)  $\eta = 0.9$ . All the radii are measured in units of  $R_{TF0}$  (outer boundary of superfluid unpolarized cloud).

of the cloud (characterized by  $R_{f2}$ ) is much larger than the superfluid cloud without population imbalance (the cloud size is measured in units of  $R_{TF0}$ ). As we increase  $\eta$ , the BP1 shell grows in size, however, size of the cloud decreases. The window of polarization for which BP1 phase forms the superfluid core starting at the center of the trap increases becoming maximum at  $\eta = 0.9$ . The BP1 phase forms the core beginning at  $P = 0.76$  in this case which should be experimentally feasible. We also present the density profiles for the same set of  $\eta$  at  $P = 0.65$  in Fig. 4.4. We note that as  $\eta$  increases, size of  $n_m$  representing density of the composite bosons shrinks but becomes more dense. It also exhibits the large cloud sizes for tightly confined minority as noted above.

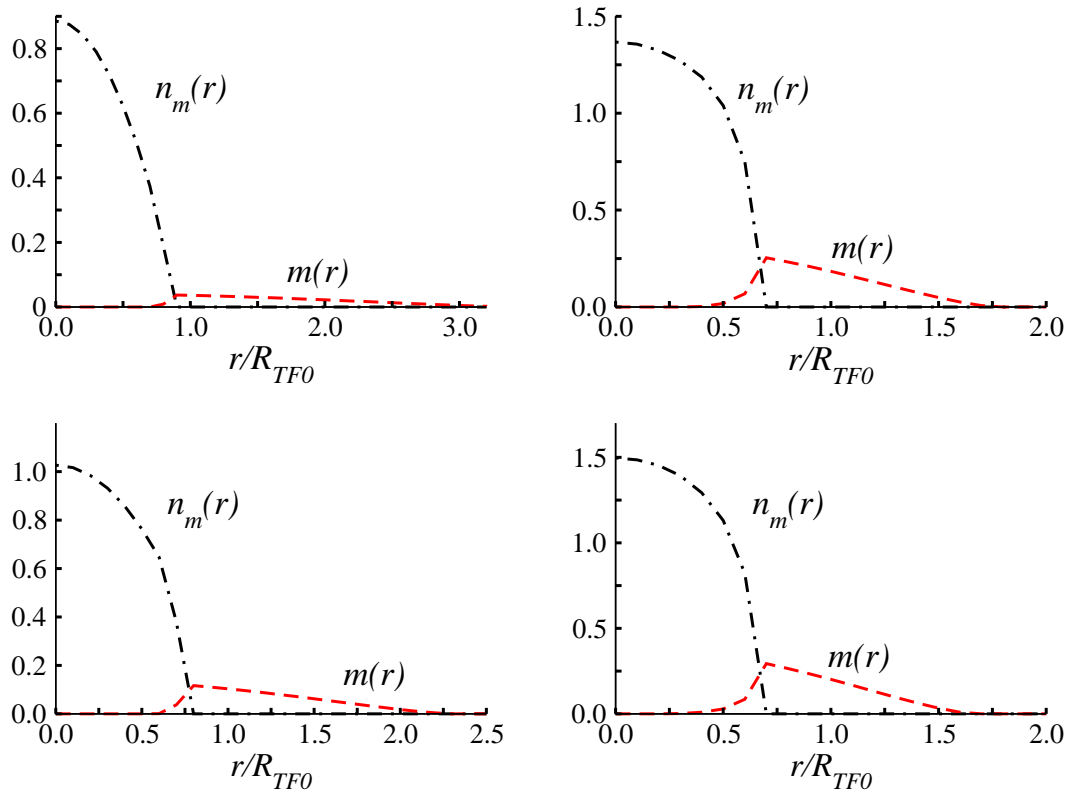


Fig. 4.4: Density profiles at  $P = 0.65$  for different values of the trap asymmetry parameter  $\eta$ . (a)  $\eta = -0.9$ , (b)  $\eta = -0.5$  (c)  $\eta = 0.5$ , (d)  $\eta = 0.9$ . The molecular density  $n_m$  and the magnetization plotted as a function of radius measured in units of  $k_F^3$  and  $R_{TF0}$  respectively.

All these features can be explained by analyzing  $(\mu(r), h(r))$  variations for each value of  $\eta$  in the phase diagram. To this end, we replot the phase

diagram enlarging the BP1 state. The line segments representing above mentioned variations are also shown (Fig. 4.5). We note that  $\eta$  with a positive (negative) value has a positive (negative) slope with zero value for  $\eta = 0$ .

Note further that BP1 to polarized N transition is second and first order for positive and negative set of chosen values respectively. These transitions can be detected via density profiles in the experiments.

The  $\eta = -0.9$  line segment traverses a small region of the BP1 phase making a second-order transition to polarized N while the  $\eta = 0.9$  segment traverses a larger region in the BP1 phase before making a first-order transition to polarized N. The order of transition can be detected in experiments via spatial discontinuities which vanish for the second-order transition. As  $\eta$  is increased from  $\eta = -0.9$  the line segments increasingly have a larger portion in the BP1 region. This explains why the BP1 shell expands in size as  $\eta$  is increased. Note further that owing to their negative (positive) slopes,  $\eta$  with negative values have longer (shorter) excursion into the polarized N state before encountering the vacuum explaining the larger (smaller) size for their clouds. Since all the atoms are integrated across the trap to conserve the atoms, the corresponding atom density distributions are also affected accounting for an increased (reduced) number of atoms in BP1 phase for  $\omega_{\uparrow} > \omega_{\downarrow}$  ( $\omega_{\uparrow} < \omega_{\downarrow}$ ).

#### 4.4 Summary

We have studied the asymmetrically trapped and population imbalanced two-components Fermi gas in the strongly attracting BEC limit at  $T = 0$ . Using the local density approximation (LDA), we calculated the shell radii of various phases in the trap as a function of polarization and trap asymmetry. Compared to symmetric trap case ( $\eta = 0$ ), we find that when the majority component is tightly confined the gapless superfluid shell (BP1) increases in size. The polarization threshold to form the BP1 superfluid at the core

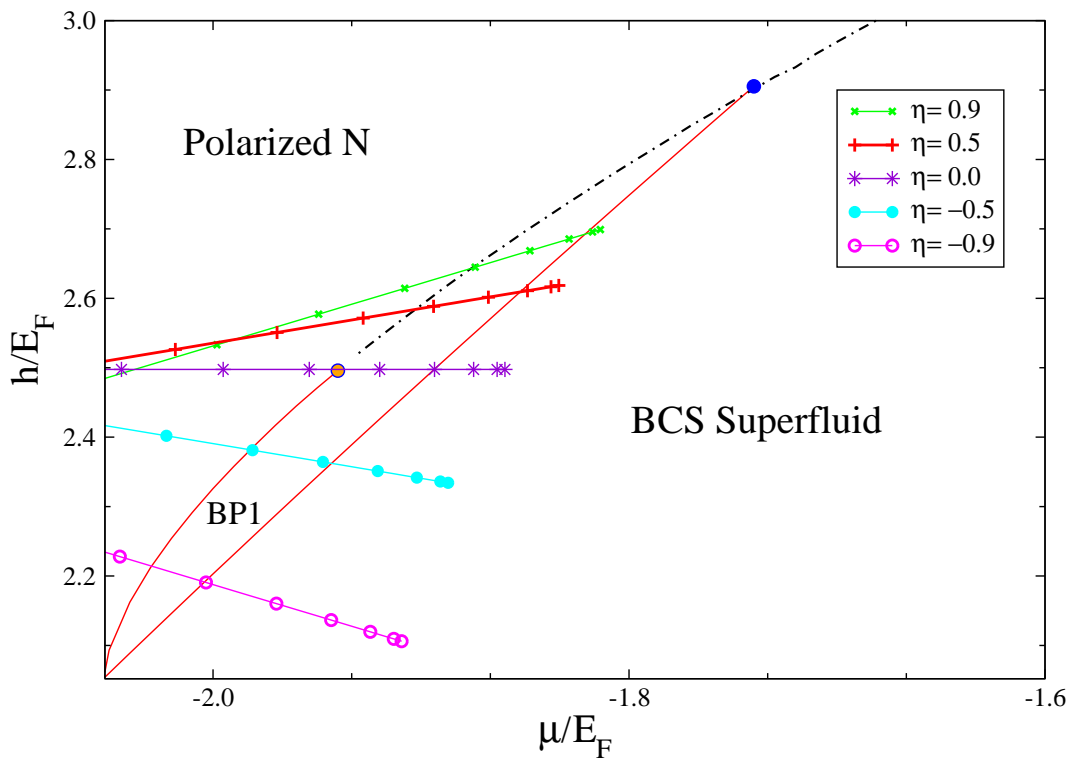


Fig. 4.5: The part of phase diagram with the BP1 region enlarged. The solid (red) line indicates the second-order phase transition and dot-dashed (black) line shows first-order transition. Superimposed are the  $\mu$ - $h$  variations as line segments for various values of the trap asymmetry parameter  $\eta$  at  $P = 0.65$ .

is reduced for a given interaction strength in this case. However, when minority are tightly confined unpolarized superfluid is favored with BP1 phase forming a narrow shell. We have explained these features using the phase diagram.

## Chapter 5

# Conclusion and Future Directions

### 5.1 Conclusion

In this thesis, we have studied the superfluid pairing in two-component degenerate atomic Fermi gas. The atomic Fermions interact via four fermion point interaction. Alongwith with the usual BCS-BEC crossover physics, we have also considered BCS pairing with mismatched Fermi surfaces. This mismatch can be introduced by population imbalance between the pairing components having two components with different masses or both.

This mismatched Fermi system is proposed to admit exotic pairing phases. However, in this thesis, we only considered breached pairing phase (BP). The BP state phase separate in momentum space with excess fermions occupying the negative quasi-particle energy states.

We have considered a variational ground state for the system of nonrelativistic fermions with a four fermion point interaction to model the phase structure of the ultracold atomic Fermi mixture. The temperature effects are taken into account by thermal Bogoliubov transformation. The stability of the solutions is decided by comparing the thermodynamic potentials of the paired state and normal matter.

We first considered the equal mass population imbalanced case and found that breached pair with one Fermi surface is stable in the BEC regime. However, it is stable only up to some critical polarization  $P_c$  for a given inter-

action strength  $(k_F a)^{-1}$  beyond which it becomes unstable to normal state.

We would like to remark here that, with a mismatch in chemical potential  $\delta_\nu$ , BCS phase is stable for value of  $\delta_\nu$  up to  $\delta_\nu = \Delta_0/\sqrt{2}$  in the weak coupling regime. This, so called Clogston-Chandrasekhar limit (21; 22), can increase as one approaches the strong coupling regime. However in this phase, there is no population imbalance.

With mass asymmetry taken into account, that is, when the two components have unequal mass, the stability region is affected. For heavier atoms as the majority component, stability threshold for BP1 phase further shifts into BEC regime being stable for large values of  $(k_F a)^{-1}$  compared to equal mass case. In contrast, for lighter atoms as majority component, it decreases and BP1 phase becomes stable at lower values of  $(k_F a)^{-1}$ .

To connect the work with the experiments, we consider the trapped Fermi mixture and include the trap effect under local density approximation (LDA) using isotropic harmonic potential. For trapped fermion with population imbalance, we obtained the shell like structure with superfluid surrounded by normal matter. The profile also show that they are mixed into each other characterizing breached pair phase.

We then study equal mass population imbalanced two-component atomic Fermi gas with unequal trap frequencies ( $\omega_\uparrow \neq \omega_\downarrow$ ) at zero temperature. Using the local density approximation (LDA), we calculated the shell radii of various phases in the trap as a function of polarization and trap asymmetry. Compared to symmetric trap case, we find that when the majority component is tightly confined, the gapless superfluid shell (BP1) increases in size. The polarization threshold to form the BP1 superfluid at the core is reduced for a given interaction strength in this case. However, when the minority is tightly confined unpolarized BCS superfluid is favored with the BP1 phase forming a narrow shell. We have explained these features using the phase diagram.

## 5.2 Future Directions

The variational method considered here using an explicit construct of the ground state, corresponds to the mean field approximation of the conventional approach. This treatment is reasonable for zero temperature and coupling away from the unitarity limit. However, the effects of the fluctuations will be important for higher temperature particularly  $T$  close to transition temperature  $T_c$ . This fluctuation was first taken into account by Nozieres and Schmitt-Rink (76) using diagrammatic perturbation theory. The functional integral approach to the problem was introduced by Sá de Melo (63) and later extended in (77) including feedback of quantum fluctuation in the gap equation. This approach recovers the  $T = 0$  and finite temperature effect within same formalism.

The future work may include application of this formalism to breached pairing phase which is stable in the BEC limit where fluctuation correction are particularly important. One can also generalize to the mass asymmetric case and the efforts in this direction have already been started (54).

We might note here for the relativistic case, inclusion of the condensate fluctuation have been attempted in (78) for the ground state that contains the fermionic condensate as well as the quanta of condensate field.

For the trapped systems, we have considered only equal mass case. The trap anisotropy together with mass asymmetry can be investigated which may exhibit rich shell structure depending on polarization, mass and trap frequency ratios. In particular, one can search for the LOFF phase where Cooper pair carries finite center-of-mass momentum (62; 79). In presence of trap anisotropy, its window of stability can be affected.

Recently zero-temperature phase structure of a two-dimensional two-component atomic Fermi gas with population and mass imbalance in the regime of the BEC-BCS crossover was explored including the possibility of LOFF phase (80). Similar study without mass imbalance but with trap

anisotropy can be carried out and fate of various phases in two dimension can be investigated.

The phase diagram for equal mass population imbalanced system in optical lattice was considered in (81). It was found that the LOFF window, i.e., the range of chemical potential imbalance within which LOFF phase is stable, increases considerably in this situation. The same system can be further probed with trap anisotropy which can affect the topology of the phase diagram. Furthermore, the mass asymmetric systems in the optical lattice can be explored.

## Publications

- Pairing in spin polarized two-species fermionic mixtures with mass asymmetry  
**S. A. Silotri**, D. Angom, H. Mishra and A. Mishra,  
*Eur. Phys. J. D* **49**, 383-390 (2008).
- Trap- and population-imbalanced two-component Fermi gas in the Bose-Einstein-condensate limit  
**S. A. Silotri**,  
*Phys. Rev. A* **81**, 013623 (2010).

# Bibliography

- [1] I. Bloch, J. Dalibard, and W. Zwerger, “Many-body physics with ultracold gases,” *Rev. Mod. Phys* **80**, 885 (2008).
- [2] S. Giorgini, L. P. Pitaevskii, and S. Stringari, “Theory of ultracold atomic Fermi gases,” *Rev. Mod. Phys* **80**, 1215 (2008).
- [3] M. H. Anderson, J. R. Ensher, M. R. Matthews, C. E. Wieman, and E. A. Cornell, “Observation of Bose-Einstein condensation in a dilute atomic vapor,” *Science* **269**, 198 (1995).
- [4] K. B. Davis, M.-O. Mewes, M. R. Andrews, N. J. van Druten, D. S. Durfee, D. M. Kurn, and W. Ketterle, “Bose-Einstein condensation in a gas of sodium atoms,” *Phys. Rev. Lett* **75**, 3969 (1995).
- [5] J. Bardeen, L. N. Cooper, and J. R. Schrieffer, “Theory of Superconductivity,” *Physical Review* **108**, 1175 (1957).
- [6] L. N. Cooper, “Bound Electron Pairs in a Degenerate Fermi Gas,” *Physical Review* **104**, 1189 (1956).
- [7] M. Houbiers, R. Ferwerda, H. T. C. Stoof, W. I. McAlexander, C. A. Sackett, and R. G. Hulet, “Superfluid state of atomic  ${}^6\text{Li}$  in a magnetic trap,” *Phys. Rev. A* **56**, 4864 (1997).
- [8] F. Dalfovo, S. Giorgini, L. P. Pitaevskii, and S. Stringari, “Theory of

- Bose-Einstein condensation in trapped gases,” *Rev. Mod. Phys* **71**, 463 (1999).
- [9] C. J. Pethick and H. Smith, *Bose-Einstein Condensation in Dilute Gases* (Cambridge University Press, 2001).
- [10] B. De Marco and D. S. Jin, “Onset of Fermi Degeneracy in a Trapped Atomic Gas,” *Science* **285**, 1703 (1999).
- [11] T. Bourdel, J. Cubizolles, L. Khaykovich, K. M. Magalhães, S. J. Kokkelmans, G. V. Shlyapnikov, and C. Salomon, “Measurement of the Interaction Energy near a Feshbach Resonance in a  $^6\text{Li}$  Fermi Gas,” *Phys. Rev. Lett* **91**, 020402 (2003).
- [12] K. M. O’Hara, S. L. Hemmer, M. E. Gehm, S. R. Granade, and J. E. Thomas, “Observation of a Strongly Interacting Degenerate Fermi Gas of Atoms,” *Science* **298**, 2179 (2002).
- [13] M. Greiner, C. A. Regal, and D. S. Jin, “Emergence of a molecular Bose-Einstein condensate from a Fermi gas,” *Nature* **426**, 537 (2003).
- [14] S. Jochim, M. Bartenstein, A. Altmeyer, G. Hendl, C. Chin, J. H. Denschlag, and R. Grimm, “Pure Gas of Optically Trapped Molecules Created from Fermionic Atoms,” *Phys. Rev. Lett.* **91**, 240402 (2003).
- [15] M. W. Zwierlein, C. A. Stan, C. H. Schunck, S. M. F. Raupach, S. Gupta, Z. Hadzibabic, and W. Ketterle, “Observation of Bose-Einstein Condensation of Molecules,” *Phys. Rev. Lett.* **91**, 250401 (2003).
- [16] G. B. Partridge, K. E. Strecker, R. I. Kamar, M. W. Jack, and R. G. Hulet, “Molecular Probe of Pairing in the BEC-BCS Crossover,” *Phys. Rev. Lett* **95**, 020404 (2005).
- [17] T. Bourdel, L. Khaykovich, J. Cubizolles, J. Zhang, F. Chevy, M. Teichmann, L. Tarruell, S. J. J. M. F. Kokkelmans, and C. Salomon, “Exper-

- imental Study of the BEC-BCS Crossover Region in Lithium 6,” *Phys. Rev. Lett.* **93**, 050401 (2004).
- [18] C. A. Regal, M. Greiner, and D. S. Jin, “Observation of Resonance Condensation of Fermionic Atom Pairs,” *Phys. Rev. Lett.* **92**, 040403 (2004).
- [19] M. W. Zwierlein, C. A. Stan, C. H. Schunck, S. M. F. Raupach, A. J. Kerman, and W. Ketterle, “Condensation of Pairs of Fermionic Atoms near a Feshbach Resonance,” *Phys. Rev. Lett.* **92**, 120403 (2004).
- [20] M. W. Zwierlein, J. R. Abo-Shaeer, A. Schirotzek, C. H. Schunck, and W. Ketterle, “Vortices and superfluidity in a strongly interacting Fermi gas,” *Nature* **435**, 1047 (2005).
- [21] B. S. Chandrasekhar, “a Note on the Maximum Critical Field of High-Field Superconductors,” *Applied Physics Letters* **1**, 7 (1962).
- [22] A. M. Clogston, “Upper Limit for the Critical Field in Hard Superconductors,” *Phys. Rev. Lett.* **9**, 266 (1962).
- [23] W. V. Liu and F. Wilczek, “Interior Gap Superfluidity,” *Phys. Rev. Lett.* **90**, 047002 (2003).
- [24] G. Sarma, “On the influence of a uniform exchange field acting on the spins of the conduction electrons in a superconductor,” *Journal of Physics and Chemistry of Solids* **24**, 1029 (1963).
- [25] Larkin and Y. N. Ovchinnikov, “Inhomogeneous state of superconductors,” *Sov. Phys. JETP* **20**, 762 (1965).
- [26] P. Fulde and R. A. Ferrell, “Superconductivity in a Strong Spin-Exchange Field,” *Physical Review* **135**, 550 (1964).
- [27] R. Casalbuoni and G. Nardulli, “Inhomogeneous superconductivity in condensed matter and QCD,” *Rev. Mod. Phys* **76**, 263 (2004).

- [28] A. Sedrakian, J. Mur-Petit, A. Polls, and H. Mütter, “Pairing in a two-component ultracold Fermi gas: Phases with broken-space symmetries,” *Phys. Rev. A* **72**, 013613 (2005).
- [29] H. Caldas, “Cold asymmetrical fermion superfluids,” *Phys. Rev. A* **69**, 063602 (2004).
- [30] G. B. Partridge, W. Li, R. I. Kamar, Y. a. Liao, and R. G. Hulet, “Pairing and Phase Separation in a Polarized Fermi Gas,” *Science* **311**, 503 (2006).
- [31] M. W. Zwierlein, A. Schirotzek, C. H. Schunck, and W. Ketterle, “Fermionic Superfluidity with Imbalanced Spin Populations,” *Science* **311**, 492 (2006).
- [32] M. W. Zwierlein, C. H. Schunck, A. Schirotzek, and W. Ketterle, “Direct observation of the superfluid phase transition in ultracold Fermi gases,” *Nature* **442**, 54 (2006).
- [33] Y. Shin, M. W. Zwierlein, C. H. Schunck, A. Schirotzek, and W. Ketterle, “Observation of Phase Separation in a Strongly Interacting Imbalanced Fermi Gas,” *Phys. Rev. Lett.* **97**, 030401 (2006).
- [34] Y.-I. Shin, C. H. Schunck, A. Schirotzek, and W. Ketterle, “Phase diagram of a two-component Fermi gas with resonant interactions,” *Nature* **451**, 689 (2008).
- [35] Y.-I. Shin, A. Schirotzek, C. H. Schunck, and W. Ketterle, “Realization of a Strongly Interacting Bose-Fermi Mixture from a Two-Component Fermi Gas,” *Phys. Rev. Lett.* **101**, 070404 (2008).
- [36] D. E. Sheehy and L. Radzihovsky, “BEC-BCS Crossover in “Magnetized” Feshbach-Resonantly Paired Superfluids,” *Phys. Rev. Lett.* **96**, 060401 (2006).

- [37] T. N. de Silva and E. J. Mueller, “Profiles of near-resonant population-imbalanced trapped Fermi gases,” *Phys. Rev. A* **73**, 051602 (2006).
- [38] M. Haque and H. T. C. Stoof, “Pairing of a trapped resonantly interacting fermion mixture with unequal spin populations,” *Phys. Rev. A* **74**, 011602 (2006).
- [39] D. T. Son and M. A. Stephanov, “Phase diagram of a cold polarized Fermi gas,” *Phys. Rev. A* **74**, 013614 (2006).
- [40] K. B. Gubbels, M. W. J. Romans, and H. T. C. Stoof, “Sarma Phase in Trapped Unbalanced Fermi Gases,” *Phys. Rev. Lett.* **97**, 210402 (2006).
- [41] W. Yi and L.-M. Duan, “Detecting the Breached-Pair Phase in a Polarized Ultracold Fermi Gas,” *Phys. Rev. Lett.* **97**, 120401 (2006).
- [42] W. Yi and L.-M. Duan, “Trapped fermions across a Feshbach resonance with population imbalance,” *Phys. Rev. A* **73**, 031604 (2006).
- [43] W. Yi and L.-M. Duan, “Phase diagram of a polarized Fermi gas across a Feshbach resonance in a potential trap,” *Phys. Rev. A* **74**, 013610 (2006).
- [44] J. Kinnunen, L. M. Jensen, and P. Törmä, “Strongly Interacting Fermi Gases with Density Imbalance,” *Phys. Rev. Lett.* **96**, 110403 (2006).
- [45] P. Pieri and G. C. Strinati, “Trapped Fermions with Density Imbalance in the Bose-Einstein Condensate Limit,” *Phys. Rev. Lett.* **96**, 150404 (2006).
- [46] K. Machida, T. Mizushima, and M. Ichioka, “Generic Phase Diagram of Fermion Superfluids with Population Imbalance,” *Phys. Rev. Lett.* **97**, 120407 (2006).
- [47] G. B. Partridge, W. Li, Y. A. Liao, R. G. Hulet, M. Haque, and H. T. C. Stoof, “Deformation of a Trapped Fermi Gas with Unequal Spin Populations,” *Phys. Rev. Lett.* **97**, 190407 (2006).

- [48] F. Chevy, “Universal phase diagram of a strongly interacting Fermi gas with unbalanced spin populations,” *Phys. Rev. A* **74**, 063628 (2006).
- [49] F. Chevy, “Density Profile of a Trapped Strongly Interacting Fermi Gas with Unbalanced Spin Populations,” *Phys. Rev. Lett.* **96**, 130401 (2006).
- [50] X. Liu, H. Hu, and P. D. Drummond, “Mean-field thermodynamics of a spin-polarized spherically trapped Fermi gas at unitarity,” *Phys. Rev. A* **75**, 023614 (2007).
- [51] M. M. Parish, F. M. Marchetti, A. Lamacraft, and B. D. Simons, “Finite-temperature phase diagram of a polarized Fermi condensate,” *Nat. Phys.* **3**, 124 (2007).
- [52] M. Taglieber, A.-C. Voigt, T. Aoki, T. W. Hänsch, and K. Dieckmann, “Quantum Degenerate Two-Species Fermi-Fermi Mixture Coexisting with a Bose-Einstein Condensate,” *Phys. Rev. Lett* **100**, 010401 (2008).
- [53] E. Wille, F. M. Spiegelhalder, G. Kerner, D. Naik, A. Trenkwalder, G. Hendl, F. Schreck, R. Grimm, T. G. Tiecke, J. T. M. Walraven, S. J. J. M. F. Kokkelmans, E. Tiesinga, and P. S. Julienne, “Exploring an Ultracold Fermi-Fermi Mixture: Interspecies Feshbach Resonances and Scattering Properties of  $^6\text{Li}$  and  $^{40}\text{K}$ ,” *Phys. Rev. Lett.* **100**, 053201 (2008).
- [54] M. Iskin and C. A. R. Sá de Melo, “Mixtures of ultracold fermions with unequal masses,” *Phys. Rev. A* **76**, 013601 (2007).
- [55] D. Blume, “Small mass- and trap-imbalanced two-component Fermi systems,” *Phys. Rev. A* **78**, 013613 (2008).
- [56] P. A. Henning, “Thermo field dynamics for quantum fields with continuous mass spectrum,” *Phys. Rep.* **253**, 235 (1995).
- [57] H. Umezawa, H. Matsumoto, and M. Tachiki, *Thermofield dynamics and condensed states* (North Holland, Amsterdam, 1982).

- [58] A. Mishra and H. Mishra, “Chiral symmetry breaking, color superconductivity, and color neutral quark matter: A variational approach,” *Phys. Rev. D* **69**, 014014 (2004).
- [59] A. Mishra and H. Mishra, “Color superconductivity and gapless modes in strange quark matter at finite temperatures,” *Phys. Rev. D* **71**, 074023 (2005).
- [60] A. Mishra and H. Mishra, “Color superconductivity with determinant interaction in strange quark matter,” *Phys. Rev. D* **74**, 054024 (2006).
- [61] B. Deb, A. Mishra, H. Mishra, and P. K. Panigrahi, “Interior gap superfluidity in a two-component Fermi gas of atoms,” *Phys. Rev. A* **70**, 011604 (2004).
- [62] A. Mishra and H. Mishra, “LOFF and breached pairing with cold atoms,” *European Physical Journal D* **53**, 75 (2009).
- [63] C. A. R. Sá de Melo, M. Randeria, and J. R. Engelbrecht, “Crossover from BCS to Bose superconductivity: Transition temperature and time-dependent Ginzburg-Landau theory,” *Phys. Rev. Lett.* **71**, 3202 (1993).
- [64] D. E. Sheehy and L. Radzihovsky, “BEC BCS crossover, phase transitions and phase separation in polarized resonantly-paired superfluids,” *Annals of Physics* **322**, 1790 (2007).
- [65] G. E. Astrakharchik, J. Boronat, J. Casulleras, Giorgini, and S., “Equation of State of a Fermi Gas in the BEC-BCS Crossover: A Quantum Monte Carlo Study,” *Phys. Rev. Lett.* **93**, 200404 (2004).
- [66] J. Carlson, S.-Y. Chang, V. R. Pandharipande, and K. E. Schmidt, “Superfluid Fermi Gases with Large Scattering Length,” *Phys. Rev. Lett.* **91**, 050401 (2003).
- [67] S. Y. Chang, V. R. Pandharipande, J. Carlson, and K. E. Schmidt,

- “Quantum Monte Carlo studies of superfluid Fermi gases,” *Phys. Rev. A* **70**, 043602 (2004).
- [68] J. Kinast, A. Turlapov, J. E. Thomas, Q. Chen, J. Stajic, and K. Levin, “Heat Capacity of a Strongly Interacting Fermi Gas,” *Science* **307**, 1296 (2005).
- [69] M. Bartenstein, A. Altmeyer, S. Riedl, S. Jochim, C. Chin, J. H. Denschlag, and R. Grimm, “Crossover from a Molecular Bose-Einstein Condensate to a Degenerate Fermi Gas,” *Phys. Rev. Lett.* **92**, 120401 (2004).
- [70] E. Gubankova, W. V. Liu, and F. Wilczek, “Breached Pairing Superfluidity: Possible Realization in QCD,” *Phys. Rev. Lett.* **91**, 032001 (2003).
- [71] M. M. Forbes, E. Gubankova, W. V. Liu, and F. Wilczek, “Stability Criteria for Breached-Pair Superfluidity,” *Phys. Rev. Lett.* **94**, 017001 (2005).
- [72] G.-D. Lin, W. Yi, and L.-M. Duan, “Superfluid shells for trapped fermions with mass and population imbalance,” *Phys. Rev. A* **74**, 031604 (2006).
- [73] M. M. Parish, F. M. Marchetti, A. Lamacraft, and B. D. Simons, “Polarized Fermi Condensates with Unequal Masses: Tuning the Tricritical Point,” *Phys. Rev. Lett.* **98**, 160402 (2007).
- [74] C.-H. Pao, S.-T. Wu, and S.-K. Yip, “Asymmetric Fermi superfluid with different atomic species in a harmonic trap,” *Phys. Rev. A* **76**, 053621 (2007).
- [75] M. Iskin and C. J. Williams, “Trap-imbalanced fermion mixtures,” *Phys. Rev. A* **77**, 013605 (2008).
- [76] P. Nozières and S. Schmitt-Rink, “Bose condensation in an attractive fermion gas: From weak to strong coupling superconductivity,” *Journal of Low Temperature Physics* **59**, 195 (1985).

- [77] R. B. Diener, R. Sensarma, and M. Randeria, “Quantum fluctuations in the superfluid state of the BCS-BEC crossover,” *Phys. Rev. A* **77**, 023626 (2008).
- [78] B. Chatterjee, H. Mishra, and A. Mishra, “BCS-BEC crossover and phase structure of relativistic systems: A variational approach,” *Phys. Rev. D* **79**, 014003 (2009).
- [79] M. Mannarelli, G. Nardulli, and M. Ruggieri, “Evaluating the phase diagram of superconductors with asymmetric spin populations,” *Phys. Rev. A* **74**, 033606 (2006).
- [80] G. J. Conduit, P. H. Conlon, and B. D. Simons, “Superfluidity at the BEC-BCS crossover in two-dimensional Fermi gases with population and mass imbalance,” *Phys. Rev. A* **77**, 053617 (2008).
- [81] T. K. Koponen, T. Paananen, J. Martikainen, and P. Törmä, “Finite-Temperature Phase Diagram of a Polarized Fermi Gas in an Optical Lattice,” *Phys. Rev. Lett.* **99**, 120403 (2007).